Results

Receptive properties of mechanoreceptors and nociceptors

To characterize the stimulus response properties of mouse cutaneous sensory neurons an *in vitro* skin nerve preparation was used to record from primary afferents of saphenous nerve. A computer-controlled device was employed to apply a standardized ramp and hold stimuli protocol and characterize the physiological properties in detail. This computer controlled mechanical stimulator enables one to precisely determine the onset of the stimulus and therefore measure the mechanical latency – the time delay between stimulus onset and the first action potential (Figure 7).

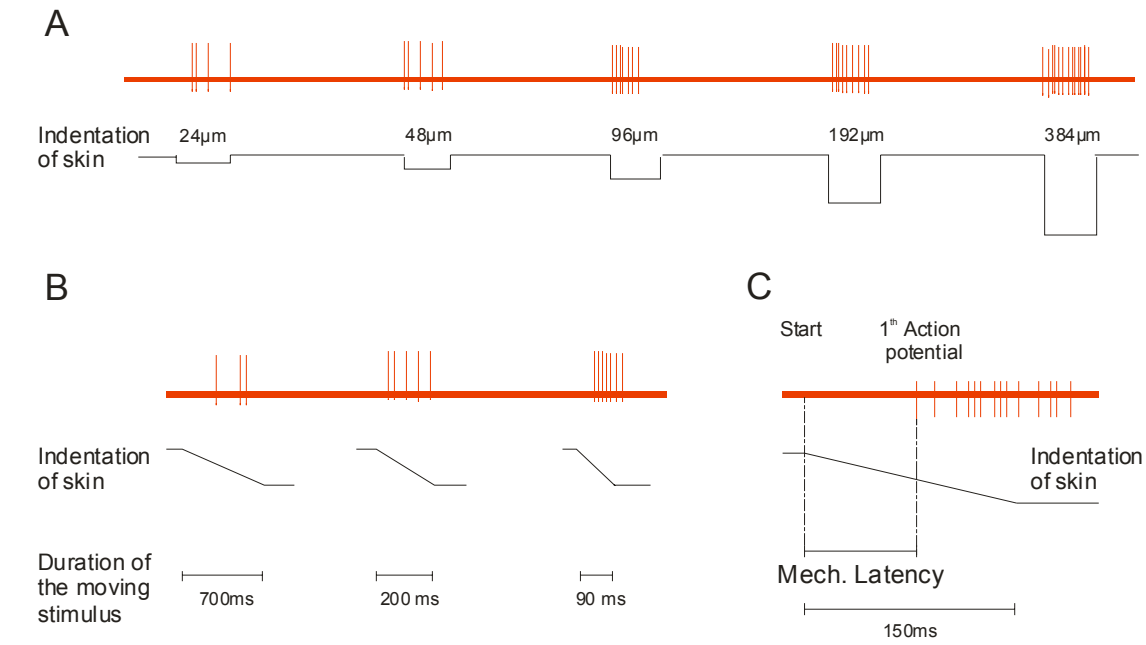

Figure 7. Schematic drawing of the mechanical parameters studied for evaluating mechanoreceptor function in mice
A The stimulus response function is produced by an ascending series of increasing displacement stimuli. B The velocity response function is generated following application of varying movement velocities. C The mechanical latency reflects the time interval from the onset of the mechanical stimulus until the first action potential is fired.

The experiments were done at two different temperatures, room (24°C) and physiological (32°C). The aim was to gain an insight into the nature of the transduction process assuming that the Q_{10} would have suggested if biochemical or physical transduction process taking place. The velocity of the moving probe could be controlled and thus, the velocity response was analyzed as well as the dependence of mechanical latency on the velocity of applied mechanical stimulus. The physiological properties were analyzed in detail for all mechanically sensitive fibers found in the saphenous nerve (Figure 1).

Mechanoreceptor sensitivity: effects of temperature

According to measured conduction velocity and receptive properties, primary afferents were classified as described previously (Koltzenburg et al., 1997; Lewin and Moshourab, 2004). The following types were distinguished: Aβ large diameter thickly myelinated low threshold mechanoreceptors, slowly (SAM) and rapidly adapting (RAM), that conduct impulses faster or equal to 10m/s; Aδ medium diameter thinly myielinated high threshold mechanoreceptors (AM) and low threshold D-hair (Dh) fibers with conduction velocities lower than 10m/s.

	32°C			***24°C***		
Receptor type	**% total**	**CV** m/s	**vFT** mN	**% total**	**CV** m/s	**vFT** mN
Aβ-fibers RAM	34.4 (32/93)	14.3±0.9	1 (0.4-1.4)	34.9 (22/63)	11.8±0.6	1.2 (1/2)
SAM	65.6 (61/93)	15.9±0.9	1.4* (1-3.3)	65.1 (41/63)	11.0±0.5	3.3* (1.3/6.7)
Aδ-fibers AM	74.1 (83/112)	5.9±0.3	3.3* (2-6.3)	75.4 (46/61)	5.0±0.4	6.3* (2.0/10.0)
Dh	25.9 (29/112)	5.4±0.36	0.4	24.6 (15/61)	3.2±0.3	0.4
C-fibers	(48)	0.51±0.03	6.3 (3.3-10)	(19)	0.38±0.04	3.3 (3.3-10)

Table 1. Detailed breakdown of the single fibre recordings from C57BL/6 mice at 32°C and 24°C

Receptor proportion (% total), conduction velocity (CV), and mechanical threshold (vFT) are shown for individual mechanoreceptor classes. There was a significant difference between SAM and AM von Fray threshold at two tested temperatures. Median values are shown with the 1st and 3rd quartile range. Means are expressed as ± s.e.m.

Unmyelinated small diameter C fiber nociceptors that have CV lower than 1m/s were also recorded. Among C-fibers two main groups were distinguished; heat sensitive (CMH) and heat insensitive (CM). In total 39 mice were used and 156 Aβ fibers (54 RAM and 102 SAM), 173 Aδ fibers (129 AM and 44 Dh), and 54 C fibers were recorded (Table 1).

Stimulus response function

For all types of fiber a standardized series of ramp and hold indentations were applied to obtain a stimulus response curve. Sequential displacements of 6, 12, 21, 48, 96, 192, 384 μm were performed at the spot determined as the center of the receptive field (Figure 8). The threshold starting point was determined by adjusting the applied displacement to the smallest that evoked a fiber to fire at least a single action potential (AP). Recordings were performed at two temperatures, 24°C and 32°C, by changing the temperature of the perfusion buffer. Two approaches were used; a single unit was recorded at both temperatures by switching the buffer temperature during the experiment, second, to exclude possible desensitization, the whole experiments were performed at one chosen temperature (24°C or 32°C). There was no difference between these two data sets and they were therefore amalgamated.

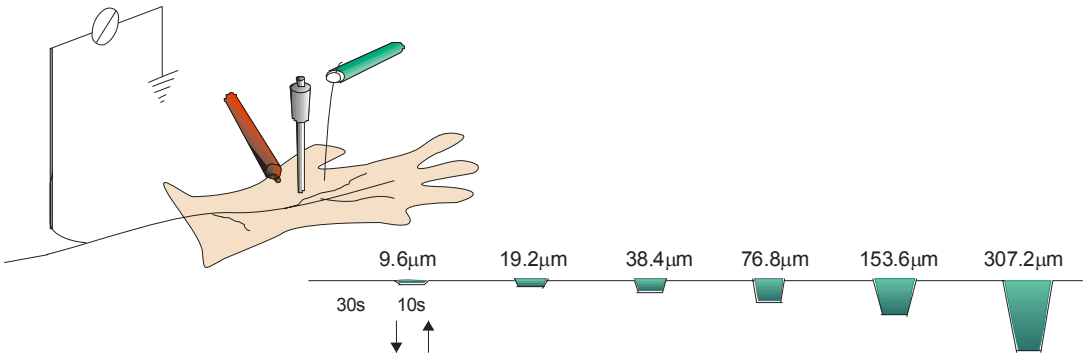

Figure 8. Standardized stimulus response protocol
The receptive field was searched using a glass rod, mechanical threshold was determined using von Frey filaments and a stimulus response recorded for standardized protocol of increasing displacements applied for 10 seconds with 30 seconds interstimulus period.

Among low threshold mechanoreceptors, SAMs respond both during the movement and static phase of stimulus, while RAMs and D-hairs code purely the phasic phase. Mechanonociceptors (AMs and mechanosensitive C-fibers) respond just to the high threshold indentation. Therefore, the phasic response was plotted for all low threshold mechanoreceptors, and total response for SAMs and mechanonociceptors. There was no significant difference between the stimulus response function recorded at 24^{o}C and 32^{o}C for all myelinated receptors (Figure 9-10), but the temperature change did influence both the firing rate and the mechanical latency of unmyelinated nociceptors (Figure 9-10).

Low threshold mechanoreceptors

D-hair receptors are the most sensitive mechanoreceptors in the skin having the lowest mechanical threshold (Burgess et al., 1968; Woodbury et al., 2001). D-hairs displayed the highest rate of firing for the lowest displacement applied, mean 71.4+12.8 spikes/second. The firing frequency stayed constant for increasing displacements (linear fit $y=a+bx$, a=61.4, b=0.007) (p=0.386, one way ANOVA) (Figure 9C).

The phasic firing frequency of Aβ fibers was similar, 49.0+9.9 spikes/s for SAMs compared to 46.3+8.8 spikes/s for RAMs, (for the 9.6 μm displacement at 32^{o}C). Because of very fast adaptation properties of RAMs the response curve gave the impression that firing frequency was lower for the greater displacement (linear fit $y=a+bx$, a=40.7, b=-0.08) (p<0.0001, one way ANOVA) (Figure 9B). One could argue that desensitization occurred, but it is more probable that it was an artifact produced by the very fast adaptation of RAMs (the duration of the displacement of 192 μm is 135 ms, and most of the units at that displacement stopped to fire after 20 ms: to calculate the rate of firing for the phasic phase the total number of spikes was divided with the duration of the movement, therefore the bigger displacements raised smaller firing frequency values). Opposite of RAM, the stimulus response curve of SAM stayed flat for greater displacements with a rising tendency (linear fit $y=a+bx$, a=57.4, b=0.17) (p<0.0001, one way ANOVA) (Figure 9A). The increase in firing rate was most probably the implication of a static component of the response which could not be avoided at longer lasting displacements. If the static component would have been excluded from the SAM firing frequencies during the phasic phase of the response its curve would most probably have been virtually flat.

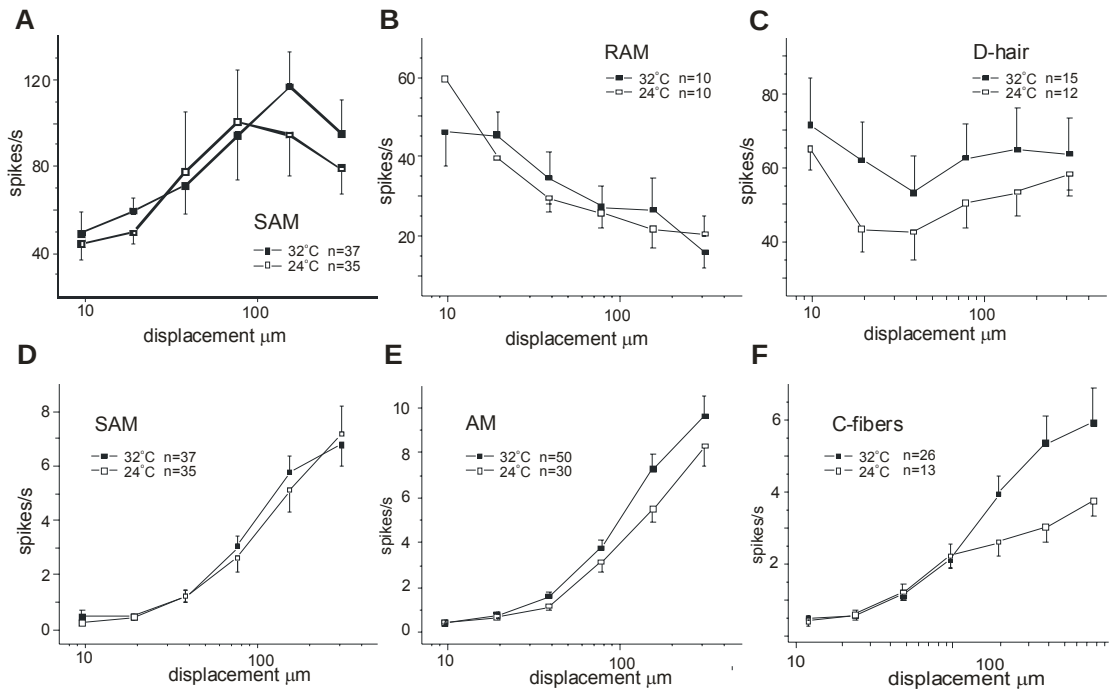

Figure 9. Stimulus response function of high and low threshold mechanoreceptors

A-B-C The phasic response of SAM, RAM, and D-hairs, respectively. D-E-F The static response of SAM, AM, and C-fibers, respectively. Note that the C-fiber stimulus response function was significantly different at two different temperatures (p=0.0419, two way ANOVA). Error bars indicate s.e.m.

Basically, all fibers with a response to the phasic stimulus (low threshold mechanoreptors) did not code the increase of applied displacement at constant velocity (1.4 m/s).

SAMs also displayed the static component of stimulus response. The maximal firing frequency for the 10 seconds stimulation was for the highest displacement performed (6.77+0.79 spikes/s at 307.2 μm) (linear fit on linear scale before desensitization $y=a+bx$, a=-0.2, b=0.04) (Figure 9D) and the stimuli higher than this lead to desensitization (data not shown).

High threshold mechanonociceptors

High threshold mechanoreceptors, Aδ nociceptors and unmyelinated C-fibers, fire during the static phase of applied displacement stimuli. AMs desensitized at stimuli higher than 400 μm, but unmyelinated nociceptor did not (experimental observation). AM fibers did

not adapt during the 10s static intendation, but rather tended to increase the firing rate. C-fibers started to code the increasing displacement over 40 μm and desensitized after indentation greater than 800 μm (Figure 9F) (not all the units were stimulated with these displacements in order to avoid desensitization in the case of paired recordings). The two types of mechanonociceptors showed different firing properties; the maximum firing frequencies for AMs were almost twice as high (9.64+0.87 spikes/s) as for unmylelinated fibers (5.89+1.00 spikes/s) (Figure 9D-F). The slope of stimulus response curve (linear fit $y=a+bx$, a=0.09, b=0.04) clearly indicated the coding properties of mechanosensitive AM fibers in this range of displacements. The stimulus response of C-fibers was influenced by the temperature. At 32°C the firing rate was significantly higher than at 24°C (p=0.0419, two way ANOVA) and this difference was observed for displacements higher than 100 μm (Figure 9F). Q_{10} of stimulus response at 400μm was 2.06 for C-fibers ($Q_8=X_{32}/X_{24}$, $Q_{10}=Q_8^{1/0.8}$). The comparison of the slope of the stimulus response curve indicates comparable coding properties of SAM and AM fibers. However, the slope of linear fit function on linear scale of C-fibers is lower, b=0.009 at 32°C, and coding abilities are even more diminished at 24°C, b=0.006.

Mechanical latency

The use of a computer controlled mechanical stimulator allowed us to record the command signal simultaneously with the receptor response and to compare them. Therefore it was possible to determine the time interval between the onset of the stimulus and the onset of the first action potential. This measure was named mechanical latency, an estimation of the time it takes a mechanotransducer to convert a mechanical signal into an action potential. Mechanical latency was characteristic for different types of mechanoreceptors.

The shortest mechanical latency was recorded for rapidly adapting fibers. On average it was 13.56+1.95 ms for RAM and 13.88+1.64 ms for D-hair fibers for 9.6 μm displacement at 1.2 m/s at 32°C (Figure 10F). As the stimuli strength increased mechanical latency increased for RAMs, but D-hairs showed no such trend (b=3E-6, p=0.226, one way ANOVA) (Figure 10B-C). This suggested that the optimal stimulus for rapidly adapting fibers was the smaller stimulus, or that the bigger displacement led to desensitization of RAMs (b=0.008 linear fit on logarithmic scale, p=0.0076, one way

ANOVA). The smallest stimulus applied that evoked the AP was one nanomotor step (0.5 μm) as recorded for some D-hair receptors (experimental observation).

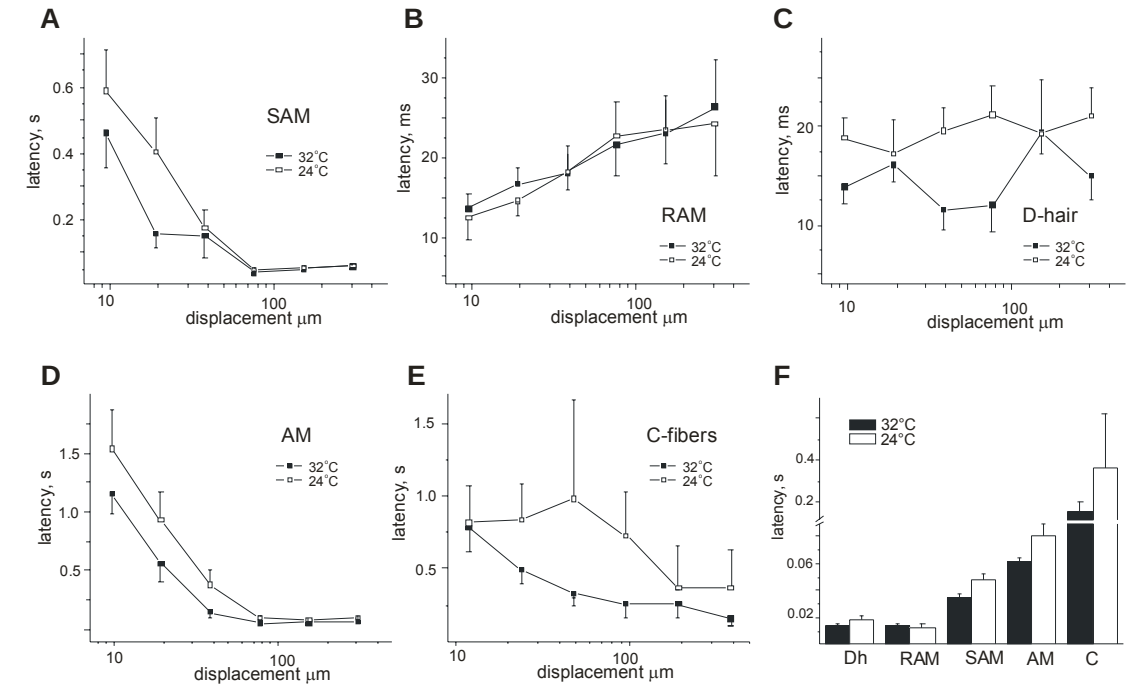

Figure 10. Mechanical latency
The mechanical latency of low threshold mechanoreceptors SAM, RAM, and D-hairs, upper row (A-B-C, respectively) and mechanonociceptors AM and C-fibers, lower row (D-E, respectively). The characteristic displacement and corresponding minimum mechanical latency are indicated with arrows for each type of receptor. Note that the C-fiber mechanical latency was significantly shorter at 32°C compared to 24°C ($p=0.0163$, two way ANOVA). F Comparison of minimal mechanical latencies for all types of mechanoreceptors at 32°C (black bars) and 24°C (white bars). Note that C-fiber nociceptors have a few times greater mechanical latency compared to myelinated mechanoreceptors. Error bars indicate s.e.m.

SAMs had longer mechanical latency compared to rapidly adapting mechanoreceptors (Figure 10F). Also, the minimum latencies were recorded at displacement characteristic for distinct types of fibers, termed characteristic displacement. The smallest mechanical latencies of SAMs were 34.18+3.65 ms and characteristic displacement was 48 μm at 32°C (Figure 10A-F). Displacements lower than 48μm did not reliably initiate phasic response of SAMs, therefore mechanical latencies for smaller displacement were relatively high and varied a lot (Figure 10A). These variations could also be depend on how precisely the stimulating probe was placed on the center of the receptive field, however, the measured mechanical latencies were characteristic of SAMs.

For AMs the mechanical latencies were significantly higher as well as the characteristic displacement, 200 μm (Figure 10D). The lowest values were 60.8+3.7 ms at 32^{o}C (Figure 10F).

The mechanical latency of any of myelinated mechanoreceptor was not influenced by temperature tested.

The only type of fiber that revealed a significant difference in mechanical latency between the two test temperatures were C-fiber nociceptors (p=0.0163, two way ANOVA). The shortest mechanical latencies were achieved at a much larger displacement compared to other mechanically sensitive units. The characteristic displacement was 400 μm and minimum mechanical latency was 153.7+47.5 ms, 10 times greater than the shortest latencies recorded for low threshold mechanoreceptive units, and almost 3 times greater then recorded for AMs (Figure 10E-F). Q_{10} of mechanical latency at 400μm was 2.95 for C-fibers ($Q_8=X_{32}/X_{24}$, $Q_{10}=Q_8^{1/0.8}$). These differences between unmyelinated and myelinated mechanoreceptors indicate that there may be a different mechanism of spike initiation after the mechanical stimuli, which might refer to characteristic ion channel expression in different receptors.

Mechanical threshold

While stimulus response function and mechanical latency were not affected by temperature, the 8^{o}C temperature difference did change the mechanical threshold of some myelinated fibers. The median von Frey threshold was 1.4mN for the SAMs at physiological temperature, while at room temperature it was increased to 3.3 mN (p=0.0197, Mann-Whitney U test) (Figure 11B). The vFT was also increased for AMs at 24^{o}C, 6.3 mN compared to 3.3mN at 32^{o}C (p=0.0240, Mann-Whitney U test) (Figure 11B). Therefore, slowly adapting myelininated fibers were susceptible to temperature decrease. SAM and AM shifted their mechanical threshold to higher values at lower temperature. The mechanical threshold of other fibers was not affected by this temperature difference.

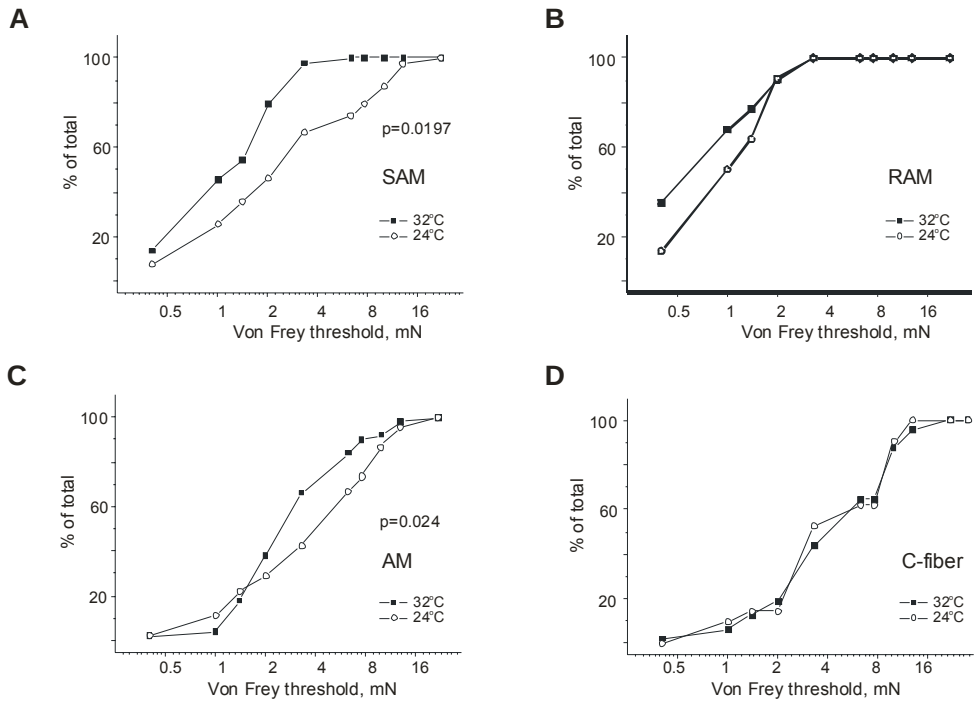

Figure 11. Von Frey threshold of mechanically sensitive receptors
vFT of low threshold mechanoreceptors, upper row, and mechanonociceptors, lower row. The typical D-hair 0.4mN vFT (0.4mN) at 32°C was not altered at 24°C. Note that SAMs (A) and AMs (C) displayed higher mechanical threshold at lower temperatures (p=0.0197, p=0.0240, respectively, Mann-Whitney U test).

Velocity sensitivity of mechanoreceptors

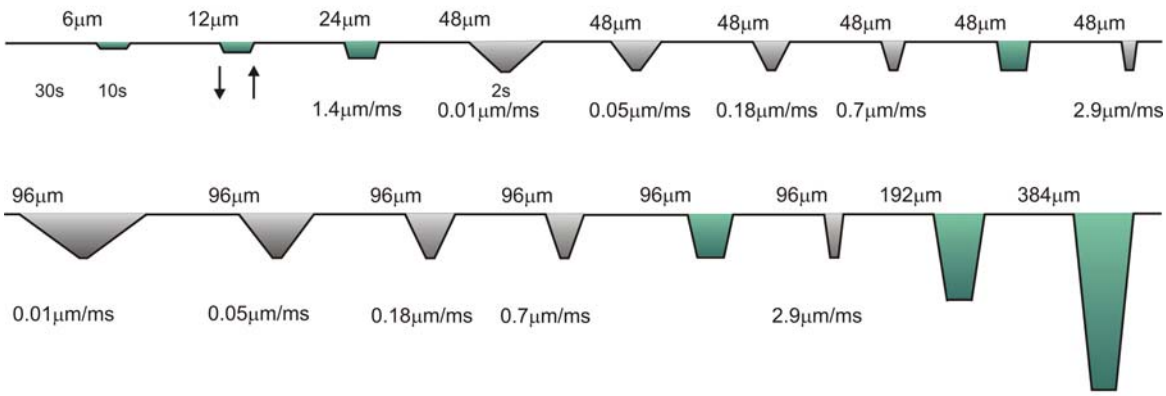

Figure 12. Standardized stimulus response protocol used to record velocity response function

The mechanosensitive units were searched and characterized as previously described. The protocol, beside the ascending series of increasing displacement, included also the velocity stimuli at two constant displacements, 48 and 96μm, depicted in gray. Five different velocity stimuli were used; 0.01, 0.05, 0.18, 0.7, and 2.9 μm/ms.

The velocity response was recorded for low threshold fibers and the phasic phase was analyzed. The steepness of the curve indicated that these fibers do code the velocity, especially rapidly adapting fibers. Compared to RAM and D-hair receptors the SAMs were the most sensitive to the slowest velocity tested: 50% of SAM responded to the velocity stimulus of 0.02 m/s with frequencies of 5 spikes/s (Figure 13A). Around 50% of D-hairs responded to the slowest movement but with the frequencies of just 0.5 spikes/s (Figure 13B). Around half of RAM fibers fired first with velocities of 0.2 m/s or greater. All low threshold fibers reached firing frequencies of 80 spikes/s for the fastest velocity tested (2.9 m/s) (Figure 13C). The slope factor of the linear fit of velocity response of SAM receptors is 32, which is much steeper than the displacement response curve.

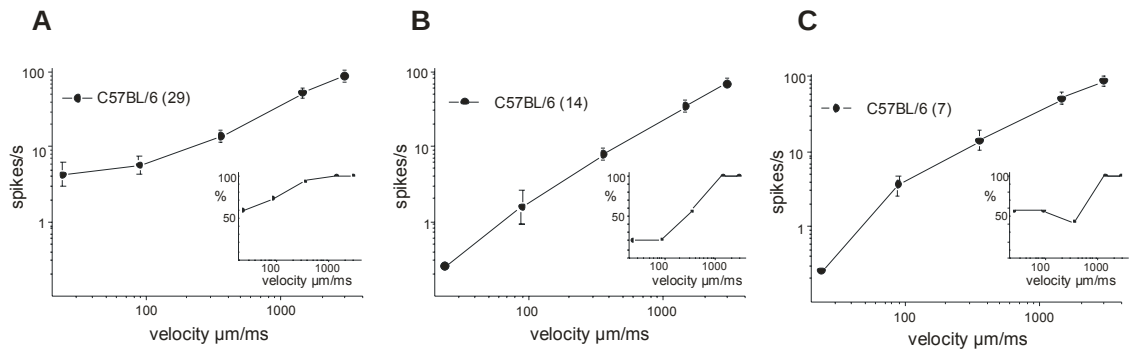

Figure 13. Velocity response function of low threshold mechanoreceptors
The velocity response function was analyzed for the ascending series of increasing velocity stimulus at constant displacement (96µm). A-B-C present SAM, D-hair, and RAM, respectively. Intercepts show the percentages of units that fired at given velocity stimuli. Error bars indicate s.e.m.

How fast could cutaneous mechanotransduction be?

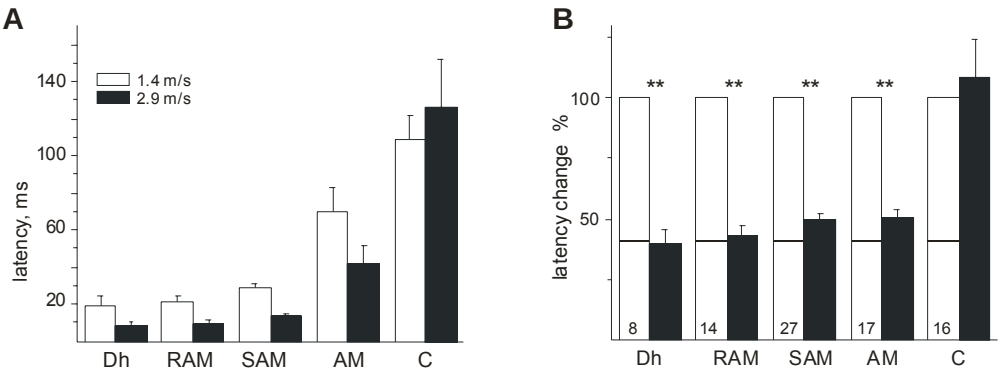

Figure 14. Mechanical latency for characteristic displacement at 1.4 and 2.9 m/s velocity of moving probe for all types of cutaneous mechanoreceptors
A The absolute values and B the change in mechanical latencies expressed as the percentage of mechanical latency at 1.4 m/s. Note the significant change for all myelinated fibers, p<0.005, <0.001, <0.001, <0.005 for D-hair, RAM, SAM, AM respectively, paired T-test. Numbers at the bottom represent the number of units analyzed. Error bars indicate s.e.m.

The standard protocol used for stimulus response function and mechanical latency function was performed at velocity of 1.4 m/s. The maximal velocity of the nanomotor

probe was 2.9 m/s. We have compared mechanical latencies for these two different velocities for the characteristic displacement for all types of fibers. For all myelinated fibers, but not for C-fiber nociceptors, mechanical latencies at 2.9 m/s were reduced to the approximately half value compared to values at 1.2m/s ($p<0.005$, <0.001, <0.001, <0.005 for Dh, RA, SA, AM respectively, paired T-test) (Figure 14). This matched with the predicted value that was calculated from the ratio of the two velocities applied - assuming that first spike appears when the threshold displacement is reached. This was not the case only for the C-fibers which did not show any significant change in mechanical latency ($p=0.3660$) (Figure 14). One could conclude that the minimum time to initiate action potential after mechanical stimulus applied at the receptive field of C-fiber mechanonociceptor was around 150 ms at 400μm displacement. Therefore, 150 ms is the lowest time limit and any faster or greater indentation could not generate receptor and action potential faster than this. Considering myelinated mechanoreceptors, the faster the movement the smaller the mechanical latency. The speed limit of the moving probe was 2.9 m/s so it was not possible to determine the minimum time these receptors need to convert stimulus into the trains of action potentials.

Summary

The characteristic response properties and mechanical latency was determined for each type of fiber. It was shown that low threshold mechanoreceptors primarily code the velocity stimuli during the phasic phase of response. The mechanosenstivity of low threshold mechanoreceptors was not altered by an 8^{o}C change in temperature. In contrast, both the stimulus response and mechanical latency are temperature dependent in C-fiber mechanonociceptors. The minimum time needed for the transduction of mechanical stimulus was revealed to be 150ms for unmyelinated fiber. The ranges of the mechanical latencies were between 10 and 30 ms for low threshold mechanoreceptors and with increasing velocity and force of the stimulus mechanical latency get shorter. The mechanosensitivity temperature dependence of C-fibers and very long mechanical latencies compared to low threshold mechanoreceptors indicate different mechanotransduction mechanisms.

Anti-NGF treatment permanently changes the phenotype of primary sensory neurons

Anti-NGF injections and determination of the effective treatment

Administration of functional blocking antibodies against nerve growth factor (NGF) during the first two weeks of postnatal life was shown to lead to phenotypic changes in primary afferents in the rat (Lewin and Mendell, 1994; Lewin et al., 1992). To test whether blocking NGF during postnatal development has similar effects in mice, subcutaneous injections of a functionally blocking antibody to NGF (anti-NGF) were performed. Three different concentrations of anti-NGF, 0.1, 0.2, and 0.5 μg/g of body weight, were used to treat neonatal mice. Anti-NGF was administrated starting from the second postnatal day (P2) until P14. Controls were injected with PBS. The effectiveness of the treatment was tested using adult treated mice by recording the proportion of Aδ fibers, low threshold D-hairs and high threshold mechanonociceptive AMs. The *in vitro* skin nerve preparation was used to record from cutaneous primary sensory neurons.

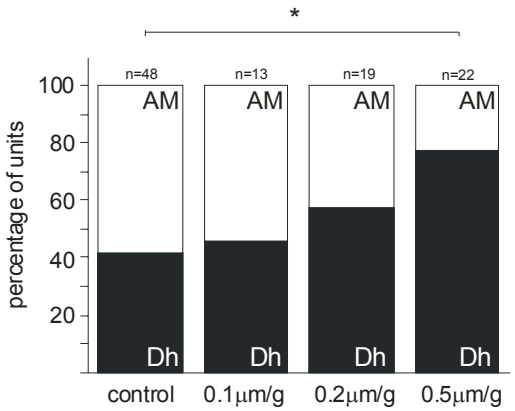

Figure 15. Determination of the effective dose of anti-NGF
The relative proportion of AM and D-hair fibers after treatment with increasing doses of anti-NGF. Note that a dose of 0.5 μg/g of body weight produced a significant effect, p=0.0215, χ^2 test.

The anti-NGF treatment led to an increased proportion of D-hair compared to AM fibers (Figure 15). Increasing dose of anti-NGF led to a more pronounced effect. The highest dose of anti-NGF produced a significant change in relative proportion of Aδ fibers ($p=0.0215$, χ^2 test). Thus, the minimal dose used in subsequent studies was 0.5 μg/g of body weight.

Characterization of anti-NGF treated mice

Mechanoreceptors and nociceptors in anti-NGF treated mice

Mechanosensitive units were found using a mechanical search stimulus. Units were probed with a glass rod to find the receptive field. The basic physiological properties of the mechanosensitive units, the conduction velocity and the von Frey threshold, were characterized. A response to a series of increasing mechanical displacements applied to its receptive field was recorded. Unmyelinated slowly conducting C fibers were additionally tested with a ramp heating stimuli.

Each anti-NGF treated group was tested to confirm that the treatment was effective. The change in relative proportion of Aδ fibers after anti-NGF treatment was recorded from at least two mice from the each treated group. Some of the treatments were not effective. In total 20 mice from anti-NGF treated group, 14 mice from control group, and 10 wt C57Bl/6 mice were used in this study. There was no difference between the wt and the control groups. The data obtained from each group was pooled.

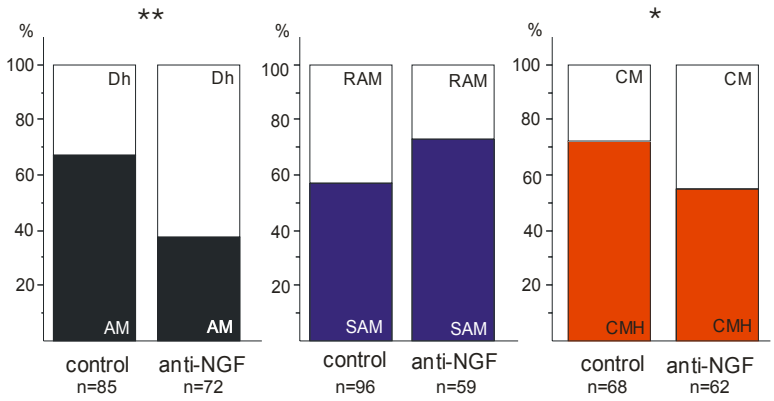

Figure 16. anti-NGF treatment during the early postnatal development induce permanent change in proportion of cutaneous sensory fibers
The change in relative proportion of Aδ mechanoreceptors (p=0.0002, χ^2 test) (left), Aβ mechanoreceptors (middle), and C-fiber mechanonociceptors (p=0.0412, χ^2 test) (right).

The proportion of the low threshold D-hairs was increased to 62.50% compared to 32.94% in control. In contrast, the proportion of AMs was reduced from 67.06% in control to 37.50% after anti-NGF treatment (p=0.0002, χ^2 test) (Figure 16). A tendency for a change in the proportion of SAM was also observed. SAM population was increased from 57.29% to 72.88% in treated group, while RAM population was decreased from 42.71% to 27.12% (Figure 16). This change in proportion did quite not reach statistical significance (p=0.0507, χ^2 test). The anti-NGF treatment induced a switch in proportion of C fibers of different modality (Figure 16). The search stimulus to isolate C fibers was probing with a glass rod. Therefore, we only recorded from C-fibers that responded to mechanical stimuli. The recorded fibers were subjected to a standard heat stimulus (preheated buffer or standardized heat ramp, see methods). Two major groups of C fibers were distinguished: presumptive polymodal C fibers that respond to mechanical and heat stimuli, CMH, and C fibers that are sensitive to mechanical stimuli but not to heat, CM (in our study this group could include some units that might also detect cooling but cold sensitivity was not systematically tested). The number of CM fibers was increased from 27.94% in control to 45.16% after anti-NGF treatment, while the percentage of CMH was reduced to 54.84% compared to 72.06% in control group (p=0.0412, χ^2 test) (Figure 16).

The proportion of Aδ fibers was changed, but the physiological properties of D-hairs and AMs were not altered (Figure 17). AM fibers were not tested for a heat response.

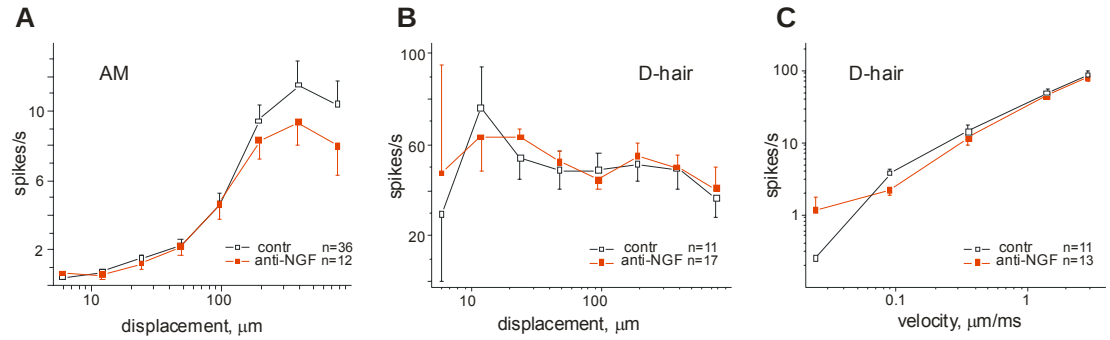

Figure 17. Mechanosensitivity of Aδ fibers after anti-NGF treatment
A, B Stimulus response function of AM and D-hair, respectively. C D-hair velocity response function. No significant differences were observed after the anti-NGF treatment for any of parameters analyzed. Error bars indicate s.e.m.

The physiological properties and mechanosensitivity of SAMs and RAMs were also not altered. There was no difference in conduction velocities, von Frey thresholds, mechanical latencies, and stimulus response curves and velocity response curves displayed the same shape and were not significantly different (Figure 18).

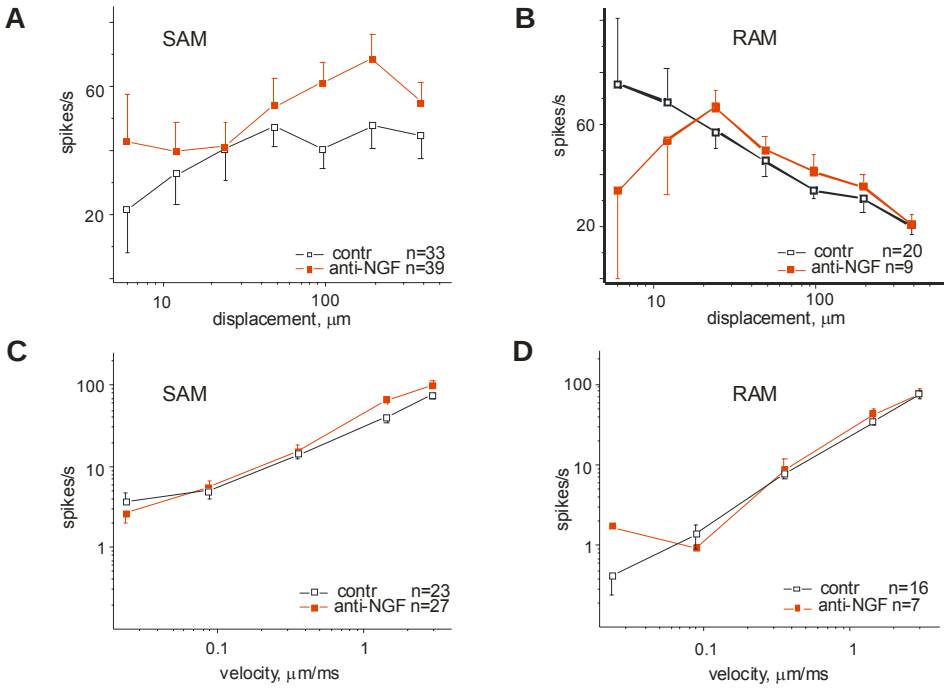

Figure 18. Mechanosensitivity of Aβ fibers after anti-NGF treatment

A, B Stimulus response function of SAM and RAM, respectively. C, D Velocity response function of SAM and RAM, respectively. No significant differences were observed after the anti-NGF treatment for any of parameters analyzed. Error bars indicate s.e.m.

C fiber stimulus response also did not show any significant difference, although there was a trend for a higher firing rate in anti-NGF treated group (p=0.192, two way ANOVA) (Figure 19A). The responses from CM and CMH fibers were also analyzed separately, as these two types of fibers could be differentially influenced by anti-NGF treatment. The neonatal anti-NGF treatment did not induce any difference in any of unmyelinated fiber types (Figure 19B-C).

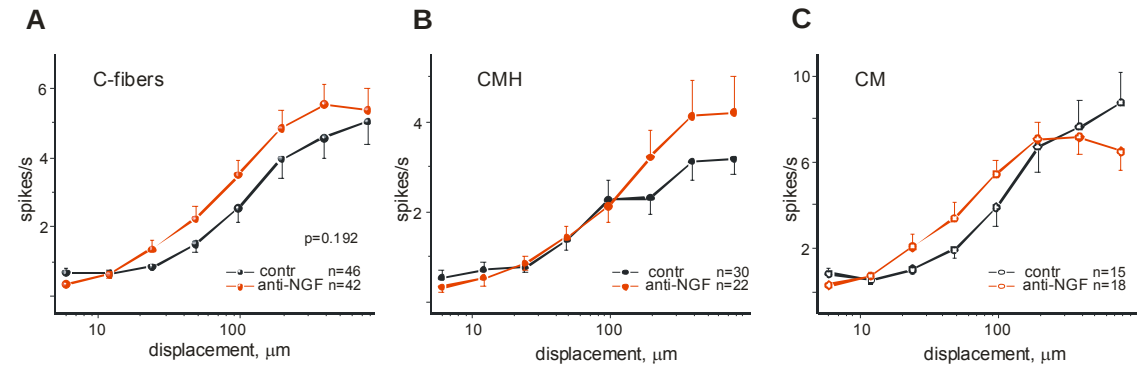

Figure 19. Mechanosensitivity of C fibers after anti-NGF treatment
A Stimulus response function of C-fibers. B, C Stimulus response function of CMH and CM, respectively. No significant differences were observed after the anti-NGF treatment. Note that C-fibers displayed a trend of higher sensitivity to mechanical stimuli after the anti-NGF treatment. Error bars indicate s.e.m.

Mechanical threshold was not different in any type of myelinated fibers. The median von Frey threshold for CMs was 10 mN in anti-NGF treated group which was significantly higher compared to 3.3 mN for the control (p=0.0028, Mann-Whitney U test). The analysis of vFT revealed that the CMs were affected by the treatment (Figure 20A).

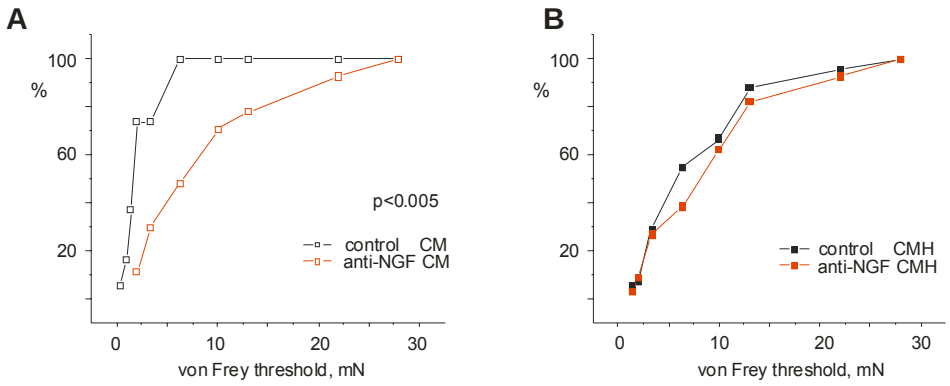

Figure 20. Mechanical threshold of C-fibers after the anti-NGF treatment
A The vFT of CM fibers was significantly higher after the treatment, p=0.0028, Mann-Whitney U test. B The treatment did not influence the vFT of CMH.

The analysis of separately plotted CMs and CMHs of treated and untreated group showed that anti-NGF did not alter the stimulus response of either group. Nevertheless, the total population of C-fibers was more sensitive to mechanical stimuli after the anti-NGF treatment. Knowing that anti-NGF treatment enriched the C-fiber population with CM at the expense of CMH, one could assume that there might be some differences in mechanical sensitivity of CM and CMH that caused the higher mechanical sensitivity in treated group. Therefore, CM and CMH were compared within both anti-NGF treated and control group.

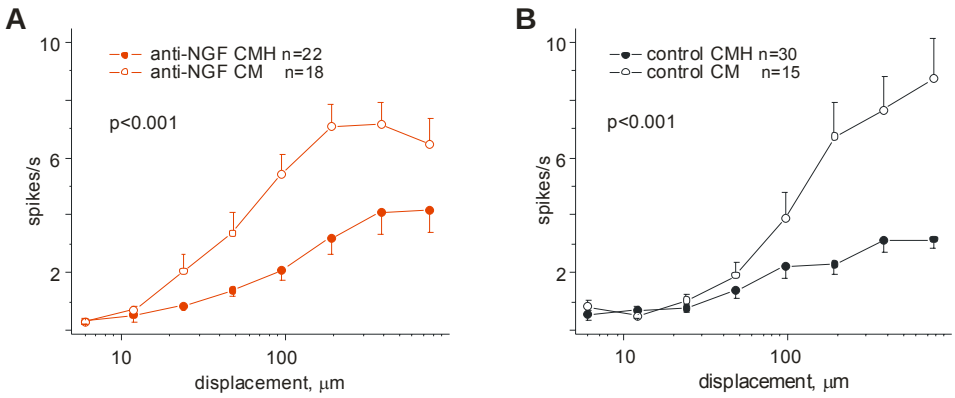

Figure 21. The comaparison of the stimulus response function of CMH and CM fibers - CM were more sensitive to mechanical stimuli compared to the CMH
A stimulus response function in control group, p<0.0001, two way ANOVA B stimulus response function in anti-NGF treated group , p<0.0001, two way ANOVA. Error bars indicate s.e.m.

In the anti-NGF group CMs had a highly significant higher firing rate compared to CMH (p<0.0001, two way ANOVA) (Figure 21A). This was also the case for the control C-fibers (p<0.0001, two way ANOVA) (Figure 21B). Thus, one could conclude that an intrinsic property of purely CM is a higher sensitivity to mechanical stimulus compared to the polymodal C fibers. There was a big difference between firing rate of CM and polymodal CMH fibers. Therefore, higher firing rate of all C fibers in the anti-NGF treated group was a direct consequence of the higher proportion of CM fibers found in this group.

Heat sensitivity after anti-NGF treatment

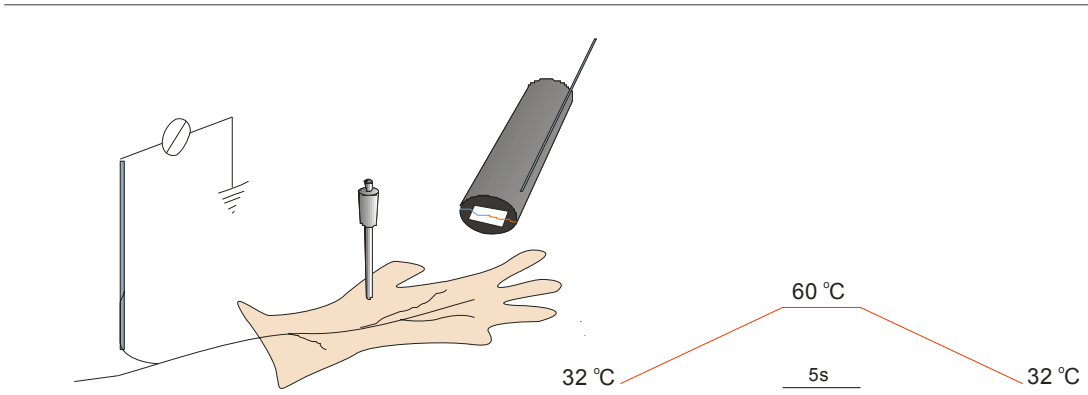

Figure 22. Standardized heating protocol
Mechanosensitive C fibers were tested for heat sensitivity. A standardized heat ramp was applied using a contact heating probe. The heat ramp started from 32°C to 60°C at the rate of 2°C/s, a constant stimulus of 60°C was used for five seconds, and then cooled down to the physiological temperature at the same rate.

The heat response of CMH fibers was investigated further in detail. A standard heat ramp stimulus was applied to single fiber, running from 32°C to 60°C at a rate of 2°C/s (Figure 22). The skin was facing the heating probe with the corium side up and free nerve endings of C-fibers terminate within epidermal layers of the hairy skin. Considering the possible discrepancy between the temperature applied and the temperature sensed by free nerve endings, an additional thermocouple was placed on the hairy side of the skin. Although some temperature difference was expected (personal communication L.M.), that was not the case, most probably because of the relatively small thickness of the skin and the relatively big size of the heating probe ($1cm^2$). In subsequent experiments only the heating probe was used to apply the stimuli and measure the temperature.

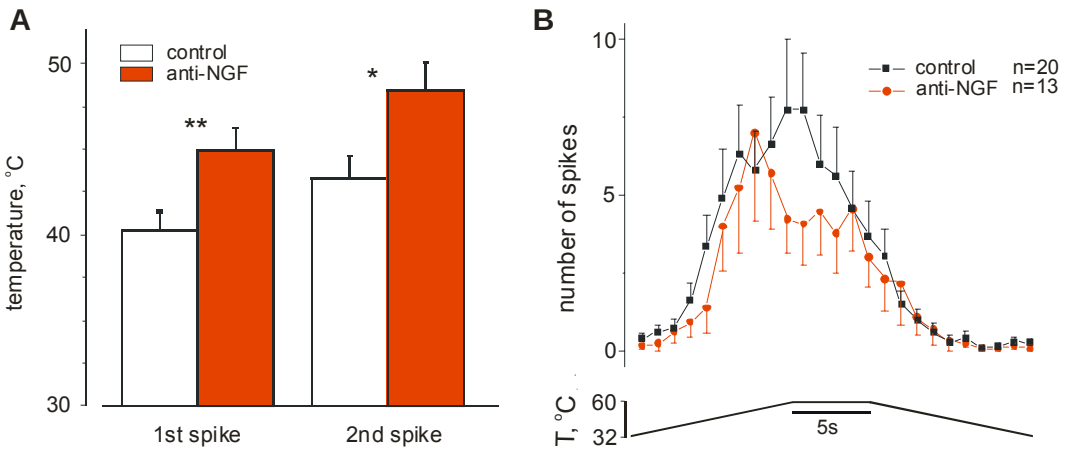

Figure 23. Effect of anti-NGF treatment on heat sensitivity of CMH
A The onset temperature for the first and the second action potential was measured for control and anti-NGF treated mice. The treatment induced the change in the thermal threshold. The threshold temperature was 5°C higher for both first (p=0.0094, unpaired t test) and the second (p=0.0144, unpaired t test) action potential after the anti-NGF treatment. B Heat response function. CMH of anti-NGF treated group displayed lower firing rate to heat ramp, but this did not reach the statistical significance. Error bars indicate s.e.m.

The temperature at which the unit fired its first action potential was measured and plotted. Considering that some C fibers show low spontaneous activity, the temperature of the onset of the second spike was also measured. There was a shift in thermal threshold of the anti-NGF treated group, both for the first and the second action potential (Figure 23A). The average temperature for the onset of the firing was 44.96+1.23°C for the anti-NGF treated mice and 40.03+1.38°C for the control group. Thus, CMH fibers in anti-NGF treated mice had a significantly higher thermal threshold of almost 5°C than found in controls (p=0.0094, unpaired t test). A similar shift in threshold temperature was also recorded for the second action potential, 48.47+1.56°C for the anti-NGF treated group compared with 43.12+1.49°C of the control mice (p=0.0144, unpaired t test). This shift of the onset of firing was obvious when the response to the entire heating ramp was recorded. The response was slightly delayed, and the total number of spikes evoked in anti-NGF mice was slightly reduced, but this did not reach the statistical significance (Figure 23B).

	control			anti-NGF		
Receptor type	**% Total**	**CV** m/s	**vFT** (mN)	**% Total**	**CV** m/s	**vFT** (mN)
Aβ-Fibers RA	42.70 (41/96)	14.94±0.55	1 (0.4-2)	27.12 (16/59)	13.20±0.64	0.7 (0,4-1,9)
SA	57.29 (55/96)	14.69±0.63	1.4 (1-3.3)	72.88 (43/59)	15.76±0.6	1 (0.85-2)
Aδ-Fibers AM	67.06 (57/85)	5.58±0.38	3.3 (2-6.3)	37.5 (27/72)	6.06±0.43	2 (1.4-3.3)
Dh	32.594 (28/85)	4.55±0.21	0.4	62.5 (45/72)	4.93±0.31	0,4
C-Fibers C-units	(68)	0.46±0.02	6.3 (3.3-10)	(62)	0.50±0.02	10 (3.3-13)
C-M	27.94 (19/68)	0.59±0.04	3.3* (2-6.65)	45.16 (28/62)	0.56±0.04	10* (3.3-13)
C-MH	72.06 (49/68)	0.45±0.02	6.3 (3.3-13)	54.84 (34/62)	0.46±0.03	10 (3.3-13)

Table 2. Detailed breakdown of the single fiber recordings from control and anti-NGF treted mice

Receptor proportion (% total), conduction velocity (CV), and mechanical threshold (vFT) are shown for individual mechanoreceptor classes. There was a significant difference between CM vFT in two groups. Median values are shown with the 1st and 3rd quartile range. Means are expressed as ± s.e.m.

Postnatal anti-NGF treatment does not induce sensory neuron death

The number of myelinated and unmyelinated axons in the saphenous nerve reflects the sensory afferent cell number. Therefore, electron microscopy was used to count all the fibers in control and anti-NGF treated mice to determine if the treatment led to a reduction in the number of neurons. Samples were taken from 4 mice per group, both nerves from left and the right side. Large myelinated axons and small unmyelinated were counted. There was no difference in the axon number in any of these groups (Figure 24). The average number of myelinated fibers (including Aβ and Aδ) was 562.8+19.3 in control and 532.3+76.7 in aNGF treated mice (p=0.853, T-test) (Figure 24B). The number of unmyelinated fibers was 2709+148.7 in control mice and slightly but not significantly reduced in aNGF treated, 2394+259.83 (p=0.344, T-test) (Figure

24B). Anti-NGF treatment did not induce the major axon loss. Change in receptor proportions was therefore most probably caused by phenotypic switch in the ganglion fiber types.

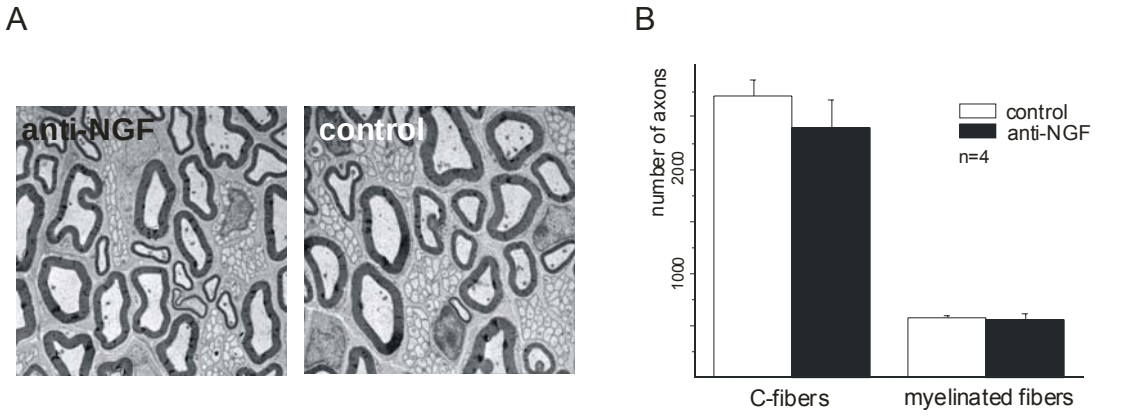

Figure 24. Electron microscopy of the saphenous nerve
A Examples of a typical electron microscopy on transverse section of saphenous nerve, anti-NGF (left) and control (right) mouse are shown. B Myelinated and unmyelinated axons were counted for a representative area of the nerve and extrapolated to the nerve cross section to determine the total number of axons in each nerve. There was no difference in the total number of axons between the genotypes neither for myelinated nor for unmyelinated fibers, p=0.853 and 0.344,respectively, unpaired t test. Error bars indicate s.e.m.

Altered pain behavior after anti-NGF treatment

Blocking NGF during a critical period in the first two postnatal weeks induced a phenotypic switch of unmyelinated fibers resulting in a decreased proportion of CMHs. The CMH fibers in anti-NGF treated mice displayed lower heat sensitivity than control. In order to see if those changes in transduction properties of fibers would be manifested at behavioral level we conducted behavioral tests. The Hardgreaves test was employed to measure the hind paw withdrawal latency; time needed to withdraw the foot that was heated with the radiant heat source. Littermate controls were used in this experiment and an equal number of males and females were tested. The experiments were carried out and analyzed blind to the treatment. The latencies for both the left and right foot were measured over period of five days and the values averaged per animal and per group. The latency for paw withdrawal was 20% longer in anti-NGF treated group compared to control group of mice (p=0.0316, unpaired t test) (Figure 25A). Withdrawal

latency was 7.22+1.49 seconds in treated and 5.92+1.54 seconds in control group. Thus, anti-NFG treated mice display heat hypoalgesia.

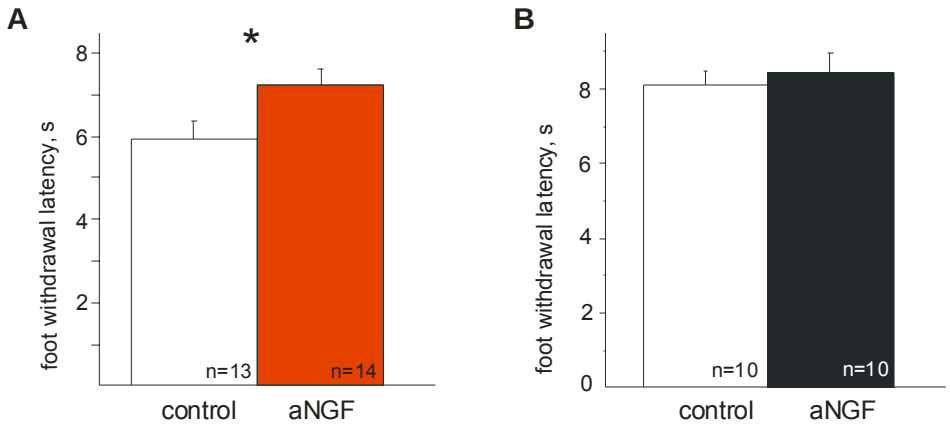

Figure 25. anti-NGF treatment led to behavioral thermal hypoalgesia
A Hardgreaves test was employed to measure the hind paw withdrawal latency. The paw withdrawal latency to noxious heat was significantly longer after the anti-NGF treatment, p=0.0316, unpaired t test. B There was no significant difference in the paw withdrawal latency to noxious mechanical stimulus. Error bars indicate s.e.m.

Since the Von Frey threshold of CM fibers was significantly higher compared to that found in control a mechanical pain test was also performed. The aestesiometer was used to test if the mechanical pain latency was changed. Littermates were used and experiments were conducted blind to the treatment. The withdrawal latency was 8.13+0.33 seconds in control and 8.41+0.57 seconds in anti-NGF treated group (Figure 25B). There was no difference in the paw withdrawal latency.

Summary

NGF signalling was blocked during the early postnatal development and this led to a permanent change in physiology of nociceptors in adulthood. Anti-NGF treatment induced the phenotypic switch of primary sensory afferents, but did not change the total neuron number in the DRG. The relative proportion of D-hairs and AM fibers was altered, while the abundance of CM fibers was increased at the expense of CMH in anti-NGF treated mice. The noxious heat sensitivity of primary sensory neurons was dramatically reduced, the heat threshold was 5^{o}C increased. The thermal hyposensitivity was also reflected at behavioral level. NGF might regulate the expression of a specific protein or group of proteins that normally confer noxious heat sensitivity on sensory neurons. Therefore, the genes with altered expression were screened after NGF deprivation using gene expression microarrays.

Changes in gene expression in the DRG after anti-NGF treatment

Screening for the regulated genes with gene chips

Anti-NGF application during the first two postnatal weeks of life induced permanent phenotypic changes in mice. The hypothesis was that the lack of anti-NGF during this critical period for the development of peripheral nervous system induced changes in the expression of genes that control the transduction properties of sensory neurons that might lead to changes in the phenotype of DRG cells. Due to the change in the abundance of receptors of different modality after the treatment, genes characteristically expressed in some of the receptors, but not under expression control of NGF, might be altered. Also NGF might directly regulate the expression of genes important for the development and transduction properties of certain receptor types. Genome chips were used to search for genes that were differently expressed after anti-NGF treatment that could be responsible for the phenotypic switch. Three experiments were carried out using DRGs from all segments and using 10 mice per group for each experiment. Labeled cRNA was hybridized to commercially available Affymetrix oligonucleotide array Mouse Genome U74B set and analysis was carried out using the Data Mining Tool software. From 36000 unique sequences represented on the chip 35% scored as present, i.e. expressed in DRG. The critical decision for the output from gene chip experiment was to choose a proper criterion for distinguishing regulated genes, 'changed' from 'unchanged'. Genes expressed in a particular cell type specifying its physiological function, could also be expressed in other types of cells that were unchanged by the treatment. Therefore, the decision was made to use relatively loose criteria for picking up regulated genes without insisting on a large fold change (change p value < 0.05). Those transcripts that were changed in the same direction in at least two out of three experiments were taken to consideration. Changes observed after anti-NGF treatment were relatively mild and did not exceed more than 30% difference compared to control. Using these criteria 141 genes were upregulated and 119 downregulated in

the anti-NGF treated group compared to control. The available data bases were screened in order to identify those genes that could be involved in the setting the phenotypic fate and physiological properties of mechanical and heat reception. Regulated transcripts, grouped by possible biological function and cellular localization are listed (Table 3).

	up	down
transmembrane ion channel	2	2
transmembrane receptor	5	6
transmembrane transporter	4	5
transmembrane	6	2
cell adhesion molecule	1	4
extracelullar secreted	6	2
neurotransmitter related	4	1
cytoskeletal binding	7	6
G protein coupled receptor	1	3
G protein signaling	2	0
signaling protein	10	7
kinase receptor	0	1
kinase	6	3
phosphatase	3	0
transpherase	5	4
synthase	1	0
Ca binding	2	1
protein transport	5	4
transcription factor	18	10
other enzymes	12	7
miscellaneous	22	17

Table 3. List of transcripts whose expression level changed after anti-NGF treatment during the critical period of postnatal development

In total, 260 transcripts changed the expression level after the treatment. Transcripts are grouped by possible biological function and cellular localization. Some of the transcripts, like ESTs, are not listed in this table.

Screening for the specific expression pattern with the large scale *in situ* hybridization

After data base screening a large sample of the regulated genes was chosen for further examination. We wanted to know if any of regulated genes exhibited a specific expression pattern in the DRG. Genes whose expression level changed could be specifically involved in setting the properties of any type of primary sensory neuron. Genes expressed in small diameter neurons, if downregulated after the anti-NGF treatment might correspond to CMHs, and if upregulated to CMs (Figure 26). Also, genes expressed in medium diameter cells, whether down or upregulated, might be AM or D-hair specific, respectively (Figure 26).

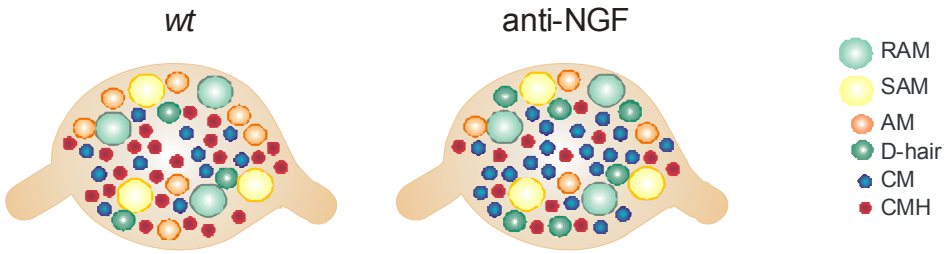

Figure 26. Schematic diagram of changes in cell population in DRG after the anti-NGF treatment
Types of cells are depicted in different colors. Note the overrepresentation of CM (blue), and D-hair (green), and under representation of CMH (dark red), AM (orange) in DRG of anti-NGF treated mouse.

The expression pattern for majority of the genes that were regulated after anti-NGF treatment was analyzed. Primers were designed for 207 transcripts, out of these 174 were successfully cloned in pGEM-T vectors for the generation of Dig labeled probes for *in situ* hybridization. *In situ* experiments, using whole mount DRGs from wild type C57BL/6 mice, showed positive staining for 69% of the probes that were screened, 20% of these clearly showed a differential expression pattern (Table 4). Considering the relatively large sample of transcripts that were checked by *in situ* hybridization, it was not insisted on optimizing the reaction by changing the reaction conditions, designing new probes or testing probes on the sections. After initial studies we focused on some of those genes that showed a specific expression pattern and for which mice carrying a null mutation were available.

	small	medium	big	unspecified
upregulated	10	5	2	
downregulated	3	4	2	
total	13 (11%)	9 (7.5%)	2 (1.5%)	96(80%)

Table 4. Tabular overview of transcripts expressed in DRG
Whole mount *in situ* hybridization was done with hybridization probes for 174 transcripts with altered gene expression after the anti-NGF treatment. 69% of these showed staining, although majority of them did not show a conclusive expression pattern. However, further work was not focused on optimization of the hybridization reaction, but on the further functional analysis of those that did clearly display specific expression pattern.

The *in situ* hybridization for some of the transcripts that showed a specific expression pattern is shown (Figure 24-39). It was possible to conclude by looking at the stained DRGs the specificity of a particular mRNA probe for a certain cell size. A semi quantitative method was therefore used to determine whether small, medium, or large cells express the gene of interest. The single cell areas were measured using MetaView software and diameter was calculated assuming that cells had a spherical shape. The cell size distribution with Gaussian fit of data for cells expressing a particular transcript were plotted.

Transmembrane channels

Serotonin and its receptors are known to be involved in nociception (Richardson, 1990). Serotonin is a major neurotransmitter component of the inflammatory chemical milieu that can be released from platelets, mast cells, or basophils that infiltrate in area of tissue damage (Dray, 1995) and interacts with a number of molecularly distinct receptor subtypes expressed by sensory terminals. **Serotonin receptor 5-HT_3** is an exctitatory channel that belongs to the nicotinic acetylcholine receptor superfamily (Maricq et al., 1991). In this study it showed downregulation upon the anti-NGF treatment which was confirmed by quantitative real time experiments (see later). It was specifically expressed in medium-diameter sensory neurons corresponding most probably to the Aδ mechanonociceptors (Figure 27). The decreased proportion of those fibers after the treatment correlates nicely with the downregulation of 5-HT_3 and its specificity for medium size cells. Analysis of 5-HT_3 mutant mice has shown no difference compared to

wt in several acute pain models including Hargreave's paw withdrawal test of thermal nociception and tail pinch test of mechanical nociception but the tissue injury induced persistent nociception was reduced (Zeitz et al., 2002).

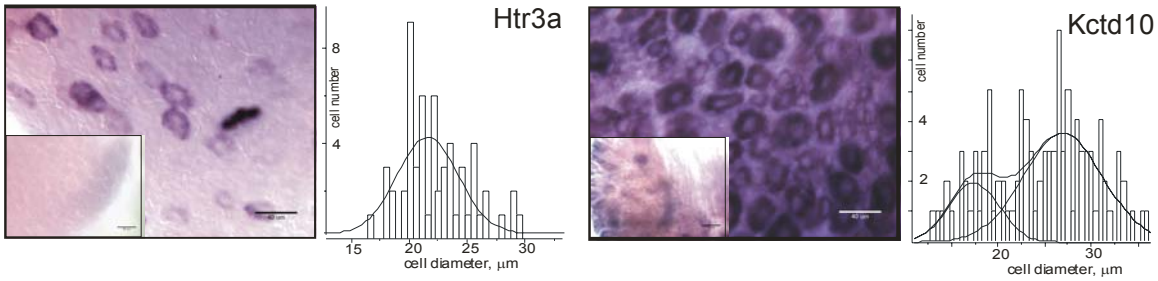

Figure 27. Specific expression pattern of transmembrane channel genes with altered gene expression after anti-NGF treatment
Whole mount in situ hybridization and cell size distribution diagram for serotonin receptor 5-HT_3 (Htr3a) (left) and tetramerization domain (T1) of voltage-gated K^+ channels (Kctd10) (right). The scale bar indicates 40 μm. The inset shows the antisense control.

Kctd10 codes cytoplasmic **tetramerization domain (T1) of voltage-gated K^+ channels**. It was found in Shaker (Kv1), Shaw (Kv3) and Shal (Kv4) subfamilies of voltage-gated K+ channel including Kv1.5, Kv3.1, Kv3.3, Kv3.4, and Kv4.1. Potassium channels are important in shaping the action potential, and in neuronal excitability and plasticity. Different subtypes of sensory neurons express different isoforms of the Kv1 subfamily. Kv1.4 is present in most small sensory neurons that express NaV1.8, while Kv1.1 and Kv1.2 are present in large-diameter sensory neurons (Rasband et al., 2001). In Affymetrix experiments the transcript was upregulated and *in situ* hybridization showed strong staining in subpopulation of big cells, and weak expression in small diameter cells (Figure 27). We did not focus on further determination of specific subtypes of potassium channels that could be specific for the certain types of cells.

Transmembrane receptors

Decay accelerating factor (Daf) is a complement regulator that functions intrinsically in the membrane of self cells to circumvent the deposition of autologous C3b on their surface and protect host cells from the consequences of complement activation (Lublin and Atkinson, 1989). It is conventionally expressed as a transmembrane (TM) polypeptide or with a post-translationally added glycosylphosphatydilinositol (GPI) anchor. Two duplicated genes Daf1 and Daf2 share 90% homology and both can be

expressed as TM or GPI anchored forms (Miwa et al., 2000). Daf2 was upregulated in the screen and *in situ* hybridization showed that it is specifically expressed in small diameter cells (Figure 28). It was previously reported that Daf2 was regulated in adult DRG cultures by application of NGF (Kendall et al., 1996) which is in agreement with our finding that its expression level is controlled by the amount of available NGF.

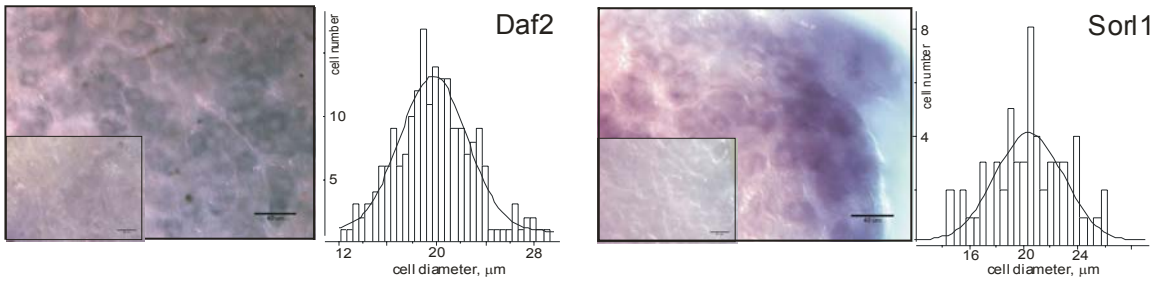

Figure 28. Specific expression pattern of transmembrane receptor genes with altered gene expression after anti-NGF treatment
Whole mount in situ hybridization and cell size distribution diagram for decay accelerating factor (Daf2) (left) and sortilin-related receptor (SorL1) (right). The scale bar indicates 40 μm. The inset shows the antisense control.

Sortilin-related receptor (SorL1) has elements characteristic of the Vps10p domain receptor family as well as the low density lipoprotein receptor family. The mammalian Vps10p-domain receptor family proteins are expressed in a number of organs but particularly in developing and adult neural tissue. The five family members are Sortilin, SorLA, and the three more recently identified receptors SorCS1–3 (Westergaard et al., 2004). SorLA was dowregulated in the screen and specifically expressed in medium diameter cells (Figure 28). This suggests that it could be specific for Aδ mechanonociceptors considering the reduction in this receptor found after anti-NGF treatment. The sorLA null mutant mouse has been studied in our lab (Hu, manuscript in preparation). There was no change in the proportion of different fibers, but slowly adapting fibers, AM and SAM, displayed increased sensitivity to mechanical stimulation. Sortilin is expressed during embryogenesis in areas where NGF and its precursor proNGF have well characterized effects (Nykjaer et al., 2004). Although not regulated in this screen, we investigated its role in primary sensory neurons and it turned out to be important in regulating the physiological properties of C fibers including both CM and CMH (Milenkovic, manuscript in preparation). Interestingly, another member of LDL

receptor family, low-density lipoprotein receptor-related protein 10 (Lrp10) was also upregulated after anti-NGF treatment.

Transmembrane proteins

Mammalian CDC50 homologs Cdc50a, Cdc50b and Cdc50c are two transmembrane-spanning proteins with one extracellular loop (Katoh and Katoh, 2004). Human *CDC50A* mRNA was expressed in embryonic stem cells, placenta, brain and chondrosarcoma. Here it was demonstrated that **transmembrane protein 30A** (Tmem30, Cdc50a) located specifically in small diameter DRG cells and was upregulated after neonatal anti-NGF treatment (Figure 29). Based on the conserved amino-acid residues and the conserved membrane topology, mammalian CDC50 homologs were predicted to be the subunits of phospholipids translocating P-type ATPases (Katoh and Katoh, 2004).

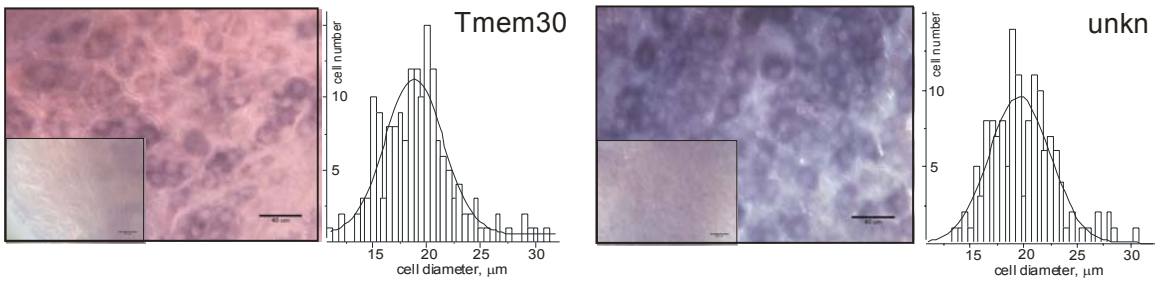

Figure 29. Specific expression pattern of transmembrane protein genes with altered gene expression after anti-NGF treatment
Whole mount in situ hybridization and cell size distribution diagram for transmembrane protein 30A (Tmem30) (left) and transcript of unknown function (unknown) (right). The scale bar indicates 40 μm. The inset shows the antisense control. The scale bar indicates 40 μm. The inset shows the antisense control.

Transcript probe 171518_i_at, named **unknown**, was upregulated in the screen and specifically expressed in small to medium diameter cells (Figure 29). Its sequence overlaps with first two exons of the epithelial membrane protein 3 (Emp3), myelin-related gene, encoding membrane glycoproteins with four trans-membrane domains.

T-cell differentiation protein 2 (Mal2) is 4 transmembrane domain-containing myelin and lymphocyte protein (MAL) belonging to MAL protein family found in the nervous system, in T-cells and some epithelial cells. It was suggested that it interacts with glycosphingolipids that are believed to decrease the permeability of lipid membranes to

small molecules and increase the ability for membrane curvature (Cheong et al., 1999). In our screen Mal2 was upregulated and expressed in medium diameter cells (Figure 30). This indicates that it may be expressed in Dh mechanoreceptors, however, considering the number of stained cells per DRG, it is most probably also expressed in other types of the cells. MAL appears to act as a TM-linker protein in T-cell signal transduction, linking the cell surface glycosyl phosphatidylinositol anchored protein CD59 to the intracellular tyrosine kinase Src (Millan and Alonso, 1998).

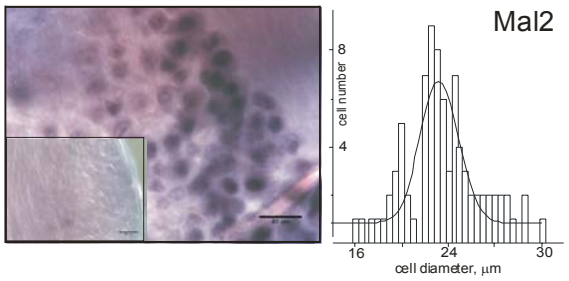

Figure 30. Specific expression pattern of transmembrane protein gene with altered gene expression after anti-NGF treatment
Whole mount in situ hybridization and cell size distribution diagram of T-cell differentiation protein 2 (Mal2). The scale bar indicates 40 μm. The inset shows the antisense control.

Neurotransmitter related

Complexins (CPLXs) are small isomeric proteins that bind to SNARE complex and modulate neurotransmitter release at the step immediately preceding vesicle fusion by regulating the exocytotic Ca^{2+} sensor or the efficiency of the fusion apparatus (Reim et al., 2001). Two isoforms of the CPLX exist in brain and the expression pattern of CPLX1 in the brain suggest its primary role in motor learning programs and sensory processing (Freeman and Morton, 2004). It was suggested that the functional role of CLPXs depends not only on the identity of neurotransmitter but also upon the circuitry connecting the neurons in which they are expressed. It was observed that **complexin 1** is expressed predominantly in medium diameter DRG cells (Figure 31). Its upregulation after anti-NGF treatment and the increased proportion of lowthreshold D-hair receptors suggests that it could be specific for this subpopulation of Aδ mechanoreceptors.

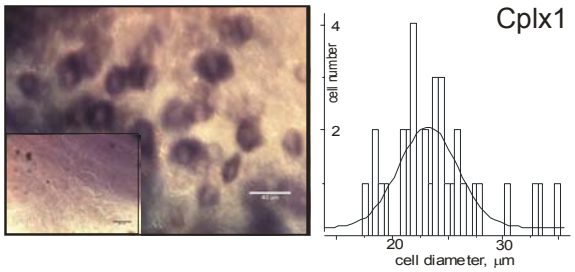

Figure 31. Specific expression pattern of neurotransmitter related gene with altered gene expression after anti-NGF treatment

Whole mount in situ hybridization and cell size distribution diagram of complexin 1 (Cplx1). The scale bar indicates 40 μm. The inset shows the antisense control.

Cytoskeletal binding

Probe 116311_at corresponds to **influenza virus NS1A binding protein** (Ivns1abp) (also known as ND1). *In situ* hybridization showed that the expression pattern is specific for small diameter cells and in Affymetrix experiments the transcript was upregulated (Figure 32). The protein contains BTB/POZ domain and Kelch domain. Some data suggest that Nd1-L functions as a stabilizer of actin filaments as an actin-binding protein and may play a role in the dynamic organization of the actin cytoskeleton (Sasagawa et al., 2002).

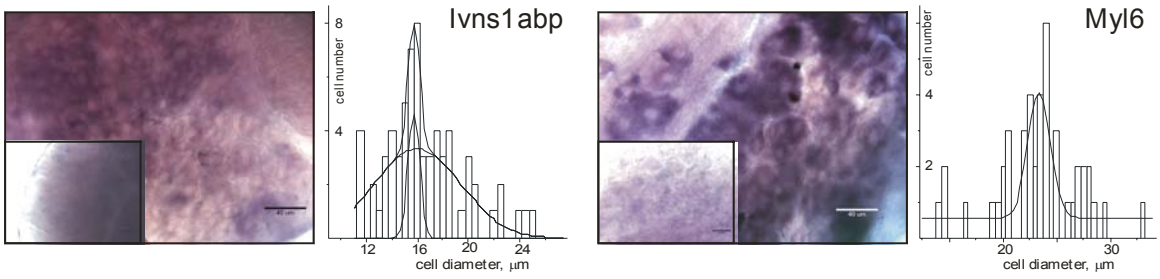

Figure 32. Specific expression pattern of cytoskeletal binding genes with altered gene expression after anti-NGF treatment

Whole mount in situ hybridization and cell size distribution diagram for influenza virus NS1A binding protein (Ivns1abp) (left) and myosin, light polypeptide 6 (Myl6) (right). The scale bar indicates 40 μm. The inset shows the antisense control.

Probe 105173_at corresponds to **myosin, light polypeptide 6** (Myl6) that was upregulated in the screen. It was expressed in different size cells, but predominantly in medium diameter cells (Figure 32). Myl6 (known as MLC3) is the smooth muscle and non-muscle specific myosin isoform, contains EFh and FRQ1 conserved calcium binding domains (Wade and Kedes, 1989).

G protein coupled receptors

At the time when the first data screening for the regulated genes after the Affymetrix gene chip experiment was done transcript 101001_at was annotated as coding for a putative 7 transmembrane protein. Now it is has been newly annotated as **G protein-coupled receptor 177** (Gpr177). This is an orphan receptor of unknown function.

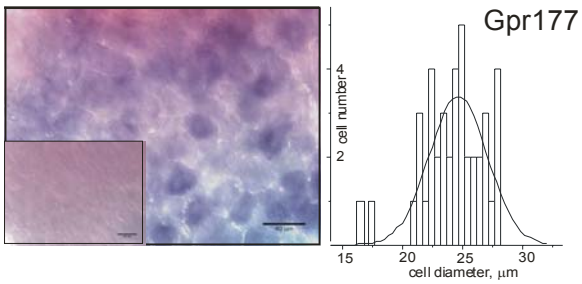

Figure 33. Specific expression pattern of GPCR gene with altered gene expression after anti-NGF treatment
Whole mount in situ hybridization and cell size distribution diagram for G protein-coupled receptor 177 (Gpr177). The scale bar indicates 40 μm. The inset shows the antisense control.

We found this gene to be expressed in the dorsal root ganglion, and *in-situ* hybridization showed that it has a specific expression pattern; it is expressed in medium diameter cells in DRGs (Figure 33). The function of this protein is completely unknown, but its expression pattern and downregulatation after anti-NGF treatment suggests that it could be involved in sensory transduction and perhaps specifically expressed in AMs. In order to gain insight into its possible functions, whether it is related to mechanotransduction or nociception, cells harboring a gene trap of Gpr177 were obtained. Insertional mutation is located in a region of the ninth exon that codes for the transmembrane domain (Figure

34). One could expect that mutation in the transmembrane domain of a GPCR would lead to its misfunction.

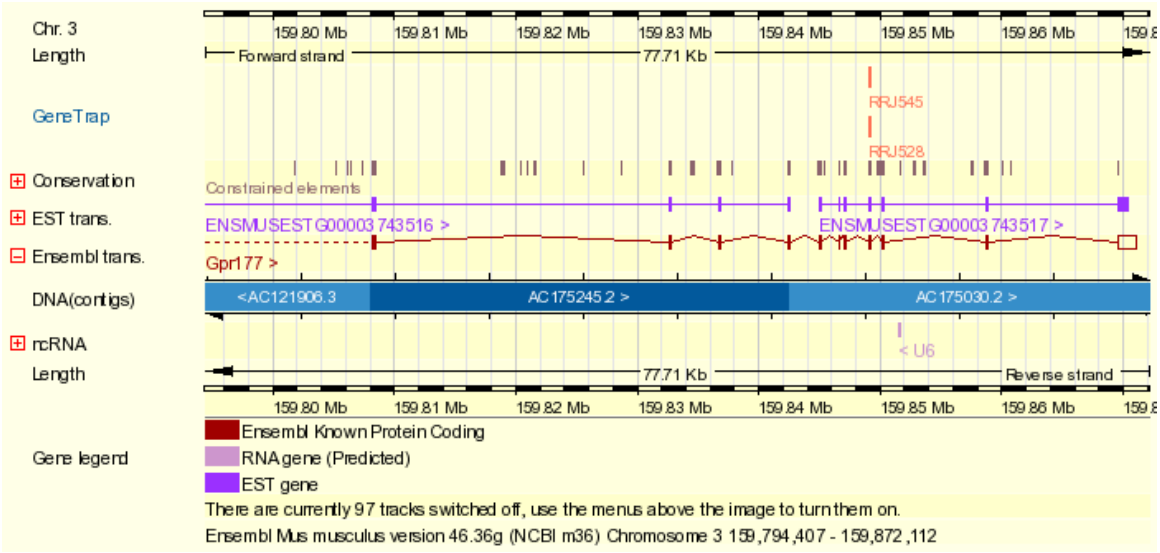

Figure 34. Detailed view of Gpr177 coding region and the position of the gene trap
(Taken from ENSEMBL).

The chimeras are born and we hope to breed a Gpr177$^{-/-}$ mouse. However, null mutants are currently not available. Being expressed in medium diameter cells suggest its putative nociceptive function and if this turns out to be the case it could lead to finding a specific target for pain treatment.

G protein signaling

Heterotrimeric G-proteins are defined by the identity of their α-subunits. The α-subunits are divided into four subfamilies based on homologies in sequence and function; $G\alpha_s$, $G\alpha_i$, $G\alpha_q$, and $G\alpha_{12}$. Each cell expresses multiple G-proteins, but each cell type contains a distinct set of G-proteins. $G\alpha_i$ proteins are involved in the inhibition of adenyl cyclases, activation of phosphoinositide 3-kinase, and activation of certain voltage-independent calcium channels (Dalwadi et al., 2003). Null mutation of the $G\alpha_{i2}$ results in a discrete and profound mucosal disorder (Rudolph et al., 1995). Although the ubiquitous expression of $G\alpha_{i2}$ has been reported, we have shown that **guanine nucleotide binding protein, alpha inhibiting 2** (Gnai2, $G\alpha_{i2}$) was specific for small diameter cells in DRGs and was upregulated after anti-NGF treatment (Figure 35). It has been shown

that $G\alpha_{i2}$ has various roles in neural tissue and our data suggest it plays a possible role in nociception.

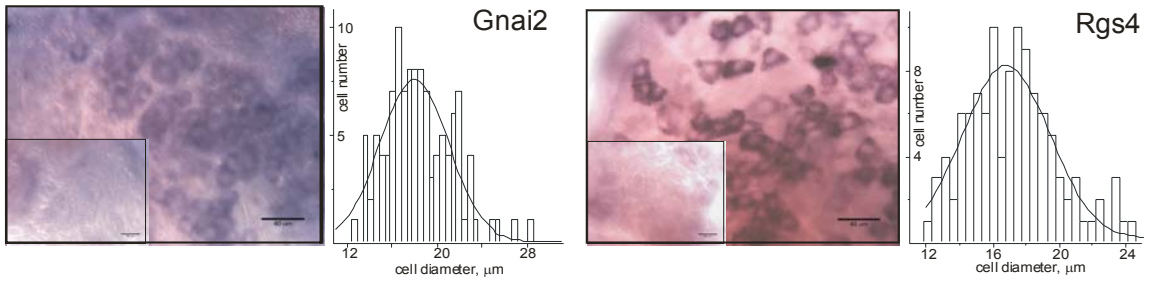

Figure 35. Specific expression pattern of G protein signaling related genes with altered gene expression after anti-NGF treatment
Whole mount in situ hybridization and cell size distribution diagram for guanine nucleotide binding protein, alpha inhibiting 2 (Gnai2, $G\alpha_{i2}$) (left) and regulator of G-protein signaling 4 (Rgs4) (right). The scale bar indicates 40 μm. The inset shows the antisense control.

Regulators of G-protein signaling (RGS proteins) increase the turn-off rate of G protein signals and inhibit signal transduction. The inhibition occurs by direct binding of RGS protein to the $G\alpha$ subunit with subsequent GTPase-accelerating protein (GAP) actions to rapidly deactivate $G\alpha$ (Berman et al., 1996) and competitively inhibit binding of $G\alpha$ effectors such as phospholipase C (Hepler et al., 1997). Null mutation of **regulator of G-protein signaling 4** (Rgs4) has subtle effect on sensorimotor function (Grillet et al., 2005). Here results confirm previously reported data that Rgs4 is expressed in a subpopulation of small diameter cells (Figure 35). Rgs4 displayed upregulation upon anti-NGF treatment. The availability of mice with null mutation of Rgs4 (kind gift of Dr. Jean-François Brunet) enabled us to further investigate its effect on heat sensitive primary sensory neurons. We performed preliminary recordings of C-fibers of *Rgs4*$^{-/-}$ mouse. Initial results are not sufficient to conclude if Rgs4 deficiency changes transduction properties of primary sensory neurons.

Signaling proteins

Ras proteins are membrane-associated molecular switches that bind GTP and GDP and slowly hydrolyze GTP to GDP. Ras activation is modulated by the local balance of guanine nucleotide exchange factors (GEFs) that stimulate the exchange of GTP for

GDP and GTPase-activating proteins (GAPs) that augment the intrinsic GTPase activity of Ras and thereby terminate signaling. **Rap guanine nucleotide exchange factor (GEF) 1** (Rapgef1) was downregulated after anti-NGF treatment and showed expression in small to medium diameter cells (Figure 36).

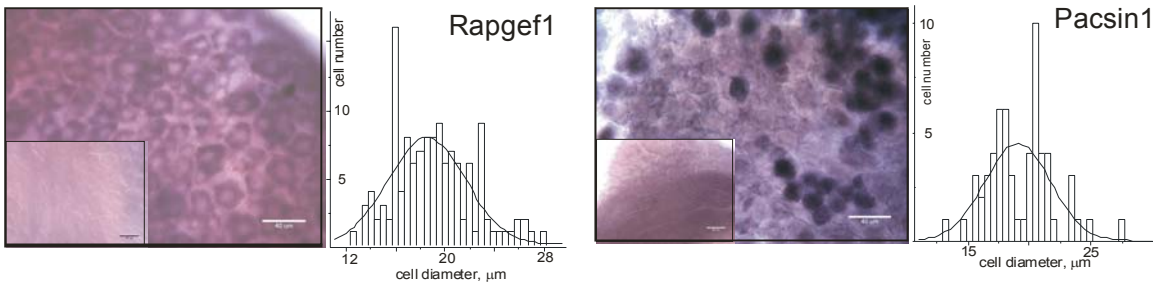

Figure 36. Specific expression pattern of signaling protein genes with altered gene expression after anti-NGF treatment
Whole mount in situ hybridization and cell size distribution diagram for Rap guanine nucleotide exchange factor (GEF) 1 (Rapgef1) (left) and Protein kinase C and casein kinase substrate in neurons 1 (Pacsin1) (right). The scale bar indicates 40 μm. The inset shows the antisense control.

PACSIN was initially identified as a brain protein that is upregulated during neuronal cell differentiation (Plomann et al., 1998). The PACSINs are a family of cytoplasmic phosphoproteins that play a role in vesicle formation and transport having general function in recruitment of the interacting proteins to sites of endocytosis (Modregger et al., 2000). **Protein kinase C and casein kinase substrate in neurons 1** (Pacsin1) is neuron specific and in our screen was scored as upregulated in the treated group by two hybridization probes present on the gene chip corresponding to this gene. *In situ* hybridization showed that it was specific for small to medium diameter DRG cells (Figure 36). It was recently shown that PACSIN1/syndapin1 was involved in the endocytic replacement of developmentally expressed NMDARs at synapses during development with mature forms (Perez-Otano et al., 2006). The pecific expression pattern, in a limited number of cells suggest that it could determine the differentiation of a subset of nociceptive CM fibers or be involved in plasticity at their central synapses.

Kinase recptor

Kit onkogene (c-Kit) was downregulated in the screen and showed a specific expression pattern. It was expressed in small diameter DRG cells and a subpopulation of big diameter DRG cells (Figure 37). The signaling of receptor tyrosine kinase c-Kit and its ligand stem cell factor (SCF) is required for the development of primordial germ cells, melanocytes, and haemopoietic lineages (mast cells and erythroid progenitors) (Besmer, 1991; Dubreuil et al., 1990). c-Kit has been shown to be highly expressed throughout the nervous system including DRGs (Keshet et al., 1991; Motro et al., 1991).

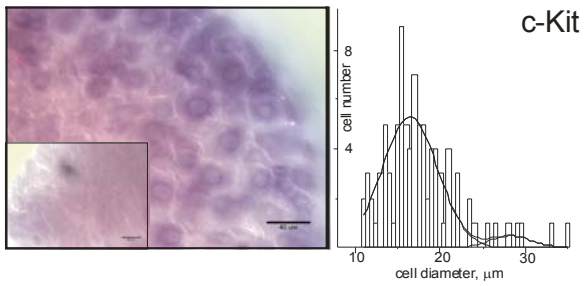

Figure 37. Specific expression pattern of kinase receptor gene with altered gene expression after anti-NGF treatment
Whole mount in situ hybridization and cell size distribution diagram of Kit onkogene (c-Kit). The scale bar indicates 40 μm. The inset shows the antisense control.

Quantitative PCR showed downregulation of *c-Kit* mRNA after the anti-NGF treatment of 23.7% (Figure 40). c-Kit function in peripheral nervous system was further studied in detail (see the following chapter).

Transferases

Sialylation plays roles in a variety of biologic processes such as cell-cell communication, cell matrix interaction, cell adhesion, and protein targeting. The transfer of sialic acids from CMP-sialic acids to the acceptor carbohydrates is catalyzed by the sialyltransferase (ST) family. Cell surface sialic acids levels are mainly correlated with the mRNA levels of ST genes (Wang et al., 2005). The expression pattern of these genes varies; the expression of some genes is restricted to certain tissues or cells or to specific stages of development (Okajima et al., 1999). **ST6**, (alpha-N-acetyl-neuraminyl-

2,3-beta-galactosyl-1,3)-N-acetylgalactosaminide alpha-2,6-sialyltransferase 5 was upregulated in all the three Affymetrix experiments. It was found to be expressed in small and medium diameter cells (Figure 38).

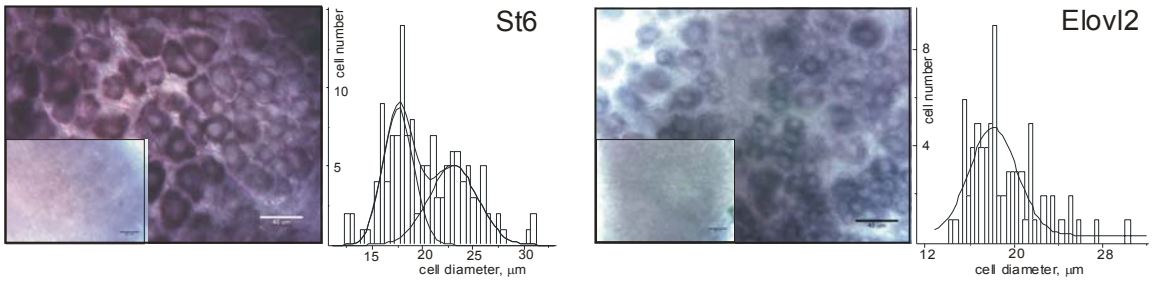

Figure 38. Specific expression pattern of transferase genes with altered gene expression after anti-NGF treatment
Whole mount in situ hybridization and cell size distribution diagram for sialyltransferase 6 (St6) (left) and Elongation of very long chain fatty acids 2 (Elovl6) (right). The scale bar indicates 40 μm. The inset shows the antisense control.

Elongation of very long chain fatty acids (FEN1/Elo2, SUR4/Elo3, yeast)-like 2 was found to be upregulated after the anti-NGF treatment. It showed expression in small diameter cells, but a few large cells were also stained (Figure 38). Members of this protein family (GNS1/SUR4 membrane protein) are involved in long chain fatty acid elongation systems that produce the 26-carbon precursors for ceramide and sphingolipid synthesis. They are predicted to be integral membrane proteins; in eukaryotes they are probably located on the endoplasmic reticulum.

Transcription factor

Probe 93054_at corresponded to transcription factor **ankyrin repeat domain 46** (Ankrd46). It was downregulated upon anti-NGF treatment and showed specific expression in medium and a subpopulation of large diameter cells (Figure 39).

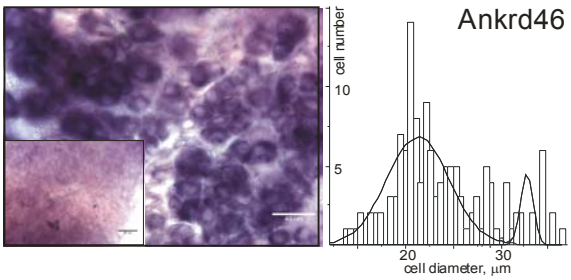

Figure 39. Specific expression pattern of transcription factor gene with altered gene expression after anti-NGF treatment
Whole mount in situ hybridization and cell size distribution diagram of ankyrin repeat domain 46 (Ankrd46). The scale bar indicates 40 μm. The inset shows the antisense control.

Confirmation of regulated genes of interest using quantitative PCR

The intention was to focus on some of the transcripts that were regulated in the Affymetrix experiments that showed specific expression patterns. Also, some of the genes were not picked up as changed by the gene chip experiment, but were previously reported to be involved in noxious heat transduction, or expressed in certain types of mechanoreceptors. Considering the relatively low reliability of gene chip experiments those transcripts were investigated using quantitative PCR (Kothapalli et al., 2002; Zirlinger et al., 2001). Genes for which the loss of function mutations in mice were already generated were of particular interest as this enabled us to test the effect of regulated genes on sensory neuron function. Some nulls of the regulated genes that were found in our screen have already been described. We were particularly interested in examining the function of novel genes that potentially contribute to the phenotype of noxious heat transduction.

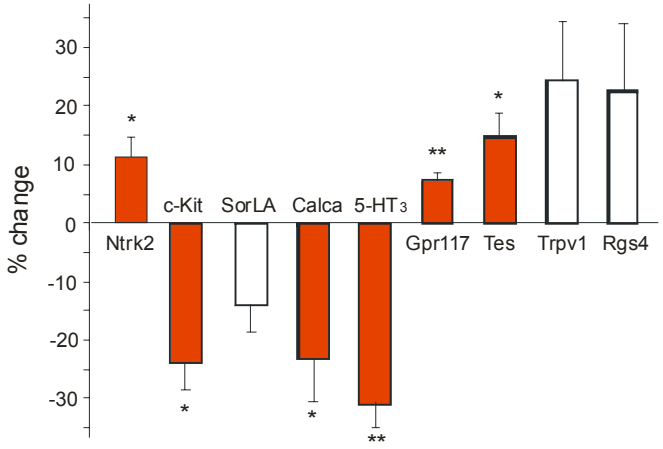

Figure 40. Gene expression change in anti-NGF treated mice relative to control
Quantitative Real Time PCR (qPCR) was used to examine the regulation of gene expression by postnatal anti-NGF treatment. Genes that might participate in sensory neuron function were examined. cDNA preparation was made from DRGs obtained from two mice per run, five runs were done for each gene. Red bars indicate statistical significance, * $p<0.05$, ** $p<0.01$. Error bars indicate s.e.m.

Ntrk2 gen codes the TrkB receptor for the brain derived neurotrophin factor (BDNF). Since TrkB is expressed in D-hairs it was expected that it would be upregulated, consistent with the increased proportion of the D-hair receptors. Indeed, Ntrk2 was upregulated, although only by 11.4% ($p=0.0423$, paired T test). We assume that, since D-hairs present only 6% of the total DRG cell population, that the expression of the transcript in the other types of the cells masked the increased number of D-hair cells expressing Ntrk2. The upregulation of **GPR177** although relatively small, 7%, was significant ($p=0.0082$). **Tes** (testis derived transcript), which encodes the protein with LIM-domain, characteristic for homeobox gene mec-3 essential for proper differentiation of the set of six touch receptor neurons in C. elegans, was upregulated by 14.7% ($p=0.0201$) (Way and Chalfie, 1988). In the future, one should further investigate its possible specificity for certain types of the cells. The upregulation of **TRPV1**, 24.4% ($p=0.0750$) and **RGS4**, 22.2% ($p=0.1315$) was not significant.

The Affymetrix **c-Kit** downregulation by 23.7% ($p=0.0237$) was confirmed. Also **Calca** (caltitonin gene related peptide) was downregulated by 23.1% ($p=0.0469$) which is consistent with recent finding that the level of expressed CGRP might influence noxious heat sensitivity (Mogil et al., 2005). **HTR3** that codes serotonin receptor and was expressed in subpopulaton of medium diameter cells was downregulated by 30.9%

(p=0.0029). The downrelation of **SorLA** of 14% did not quite reach statistical significance (p=0.0503).

Summary

Gene chip experiments revealed numerous genes with altered expression level in adult mice DRGs after postnatal anti-NGF treatment, although changes were relatively mild. An expression pattern of a large sample of 'changed' transcripts was analyzed using *in situ* hybridization experiments. Around 20 percent of hybridization probes clearly showed an expression pattern specific for a subpopulation of the DRG neurons. Some of the genes with altered expression level after temporal postnatal NGF signaling blockade and with differential expression in the DRG were already implicated to be involved in the function of the primary sensory neurons. Those include 5-HT_3 receptor and SorL1. In addition, qPCR confirmed the up/down regulation of some of the genes that were picked up by the gene chip experiment, and also showed the altered expression level of some genes that were expected to be altered according to the phenotypic changes, like *Ntrk2*. One of the interesting genes was Gpr177, a G protein coupled receptor of unknown function, and I hope to examine the possible function of Gpr177 in primary sensory neurons in the near future. Particularly interesting was the kinase receptor c-Kit, expressed in small and subpopulation of large diameter DRG neurons. The availability of *c-Kit* null mice enabled me to proceed with a detailed study of c-Kit function in sensory transduction, and the results are described in the following chapter.

Function of c-Kit in sensory transduction

c-Kit, a receptor tyrosine kinase belonging to the platelet-derived growth factor (PDGF) receptor subfamily, is encoded at the murine W locus and controls diverse cellular processes during development and in the adult animal (Chabot et al., 1988). The signaling of receptor tyrosine kinase c-Kit and its ligand stem cell factor (SCF) is required for the development of primordial germ cells, melanocytes, and haemopoietic lineages (mast cells and erythroid progenitors) (Besmer, 1991; Dubreuil et al., 1990). Allelic mutation in *SCF* or *c-Kit* gives rise to dominant white spotting pigment phenotypes and their analysis provided the first genetic evidence for an essential function of receptor tyrosine kinase signaling in mammalian development (Besmer, 1991; Little, 1915). c-Kit is highly expressed throughout the nervous system including DRGs (Keshet et al., 1991; Motro et al., 1991).

c-Kit was one of the transcripts that was downregulated in the screen and showed a specific expression pattern. It was expressed in small diameter cells and a subpopulation of big cells in DRG (Figure 37). Quantitative PCR showed downregulation of *c-Kit* mRNA after the anti-NGF treatment of 23.7% (Figure 40).

The analysis of c-Kit function was hampered due to the well known haematopoietic defect in *c-Kit*$^{-/-}$ and consequential low survival rate (Reith et al., 1990). However, the inbred mutant substrains established during intensive inbreeding regimes to select for survival of homozygote mutants enabled the analysis of adult mice completely lacking c-Kit function (Waskow et al., 2002). Nervous system phenotype has not been reported in *c-Kit*$^{-/-}$ mice. A mouse strain harboring a *c-Kit* null mutation, a point mutation in the 5' intron splice donor site downstream of the exon encoding the transmembrane domain (dominant white spotting W allele), was used in this study to investigate c-Kit function in sensory transduction (Hayashi et al., 1991; Nocka et al., 1990). In addition a mouse line caring the *c-Kit* null mutation was crossed with a transgenic mouse line overexpressing erythropoietin to increase the proportion of surviving c-Kit mutants. The breeding and lethal anemia rescue strategy was initiated and carried out by Dr. Alistair Garratt.

The same procedure was employed to investigate c-Kit function in the physiology of cutaneous primary sensory neurons as previously described for the anti-NGF treated mice.

Mechanical sensitivity in *c-Kit*$^{-/-}$

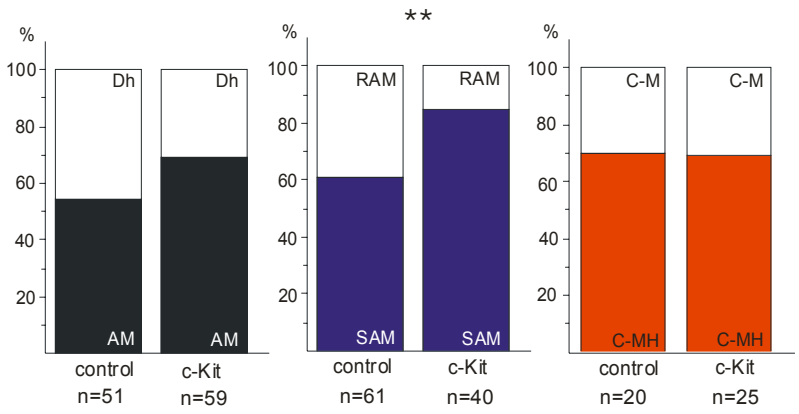

Figure 41. Mice expressing the c-Kit null mutation have an altered proportion of cutaneous sensory fibers
There was a change in relative proportion of SAM and RAM receptors. The proportion of Aδ and C-fibers were not altered. Relative proportion of Aδ mechanoreceptors (left), Aβ mechanoreceptors (p=0.0088, χ^2 test) (middle), and C-fiber mechanonociceptors (right).

All types of cutaneous sensory neurons were recorded focusing on unmyelinated nociceptors. A total of 274 mechanosensitive units, 101 Aβ fibers, 110 Aδ fibers, and 63 C fibers, were studied from the 15 *c-Kit*$^{-/-}$ and 10 *c-Kit*$^{+/+}$ adult mice (table 4). There was a change in the relative proportions of SAMs and RAMs in the Aβ fiber range (Figure 41). The proportion of SAMs was increased to 85% compared to 60.7% in *c-Kit*$^{+/+}$ mice and the RAMs proportion was reduced from 39.3% in *c-Kit*$^{+/+}$ to just 15% in *c-Kit*$^{-/-}$ mice (p=0.0088, χ^2 test). This might reflect a selective cell death of the RAM population or an altered differentiation of mechanoreceptors in the absence of c-Kit signaling. A similar shift was seen in the anti-NGF treated mice, although this change did not reach

statistical significance (p=0.0507, χ^2 test). There was nonsignificant tendency for a change in the relative proportion of Aδ fibers, the proportion of AM was reduced from 68.6% to 54.2%, and Dh increased proportion from 29.5% to 45.8% in *c-Kit*$^{-/-}$ (p=0.1230, χ^2 test). The proportion of CMH and CM unmyelinated fibers was not altered.

	control			***c-kit***		
Receptor type	**% Total**	**CV** m/s	**vFT** (mN)	**% Total**	**CV** m/s	**vFT** (mN)
Aβ-Fibers RAM	39.3 (24/61)	15.48±0.79	0.7 (0.4-1.4)	15 (6/40)	10.88±0.58*	0.4 (0,4-0.85)
SAM	60.7 (37/61)	15.11±0.87	1.4 (1-2)	85 (34/40)	11.12±0.49*	1* (0.4-1)
Aδ-Fibers AM	68.6 (35/51)	5.9±0.52	3.6 (2-6.3)	54.2 (32/59)	5.43±0.42	2.5* (1.4-3.3)
Dh	29.5 (16/51)	4.32±0.18	0.4	45.8 (27/59)	4.55±0.22	0,4
C-Fibers C-units	(29)	0.55±0.03	6.3 (3.3-10)	(34)	0.45±0.03	6.3 (3.3-10)
C-M	30 (6/20)	0.57±0.08	10 (3.3-10)	32 (8/25)	0.45±0.03	4.8 (2.32-9.07)
C-MH	70 (14/20)	0.5±0.03	6.3 (3.3-7.2)	68 (17/25)	0.47±0.03	6.3 (3.3-13)

Table 5. Detailed breakdown of the single fiber recordings from *c-Kit*$^{-/-}$ and control *c-Kit*$^{+/+}$ mice

Receptor proportion (% total), conduction velocity (CV), and mechanical threshold (vFT) are shown for individual mechanoreceptor classes. There was a significant difference between the average conduction velocity of Aβ SAM and RAM in *c-Kit*$^{-/-}$ mice (p=0.007, unpaired T test). SAM and AM von Fray thresholds were significantly reduced in *c-Kit*$^{-/-}$ mice (p=0.0002, p=0.0315, respectively, Mann-Whitney U test). Median values are shown with the 1st and 3rd quartile range. Means are expressed as ± s.e.m.

The average conduction velocity of Aβ SAM and RAM in c-Kit mutants was significantly slower than the average CV of Aβ fibers in controls (p=0.007, unpaired T test) (Table 5). The conduction velocity cut-off between Aβ and Aδ fibers was determined to be 9 m/s in *c-Kit* mutants based on measurements of the Aβ and Aδ wave in compound action potential recordings (Koltzenburg et al., 1997).

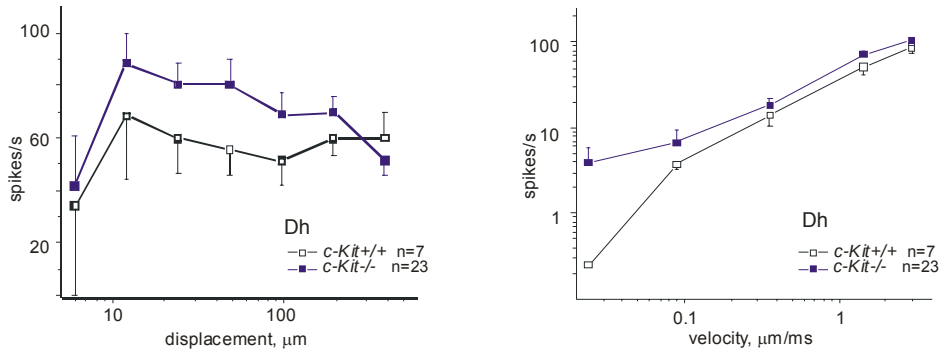

Figure 42. Mechanosensitivity of D-hairs in *c-Kit*$^{-/-}$ mice
Stimulus response function (left) and velocity response function (right). No significant differences were observed for any parameter analyzed. Error bars indicate s.e.m.

Due to a very small number of RAM units in *c-Kit*$^{-/-}$ mice it was not possible to compare the stimulus response function for this type of units between *c-Kit*$^{-/-}$ and *c-Kit*$^{+/+}$ mice. The stimulus response and mechanical latency of D-hair receptor in *c-Kit*$^{-/-}$ mice was not different compared to control (Figure 42). The stimulus response recorded from SAM was very different in *c-Kit*$^{-/-}$ compared to *c-Kit*$^{+/+}$ mice (Figure 43). SAM neurons displayed an increase in their mechanosensitivity in *c-Kit*$^{-/-}$ compared to control mice. There was a significant increase in the firing rate in *c-Kit*$^{-/-}$ mice ($p=0.0022$, two-way ANOVA); the numbers of spikes evoked by a series of displacement stimuli in *c-Kit*$^{-/-}$ mutants was twice that of SAM fibers recorded in control mice (Figure 43A). The phasic response was analyzed separately and was increased, but this did not reach statistical significance ($p=0.0585$, two-way ANOVA) (Figure 43B).

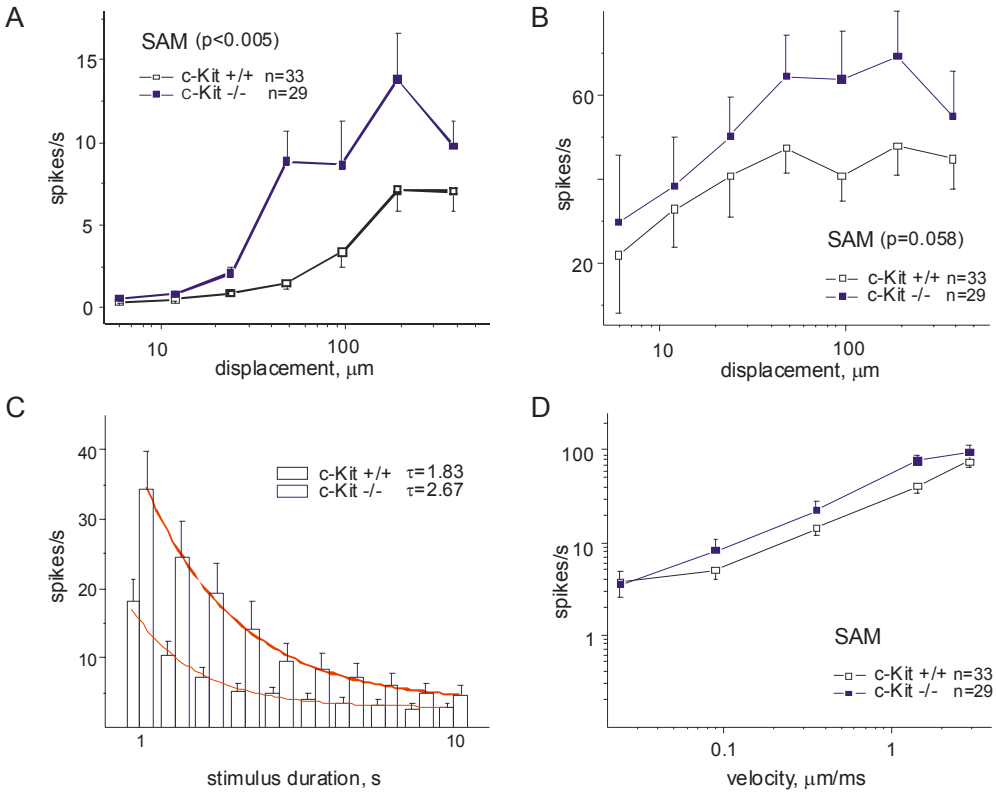

Figure 43. Mechanosensitivity of SAMs in *c-Kit*$^{-/-}$ mice
A Stimulus response function, total response (left) and phasic response (right). Firing rate of total response was significanlly increased in *c-Kit*$^{-/-}$ (p=0.0022, two-way ANOVA). B Time constant describing the lowering of firing rate of tonic phase of stimulus response was similar in *c-Kit*$^{-/-}$ and *c-Kit*$^{+/+}$. C Velocity response function. No significant differences were observed. Error bars indicate s.e.m.

The rate of firing during the 10 seconds of static indentation was plotted for SAM. To compare the adaptation during the tonic response the rate of firing for 192μm displacement was fitted with an exponential curve of first order $y = e^{-x/\tau}$, where τ describes time constant; the time firing rate take for the decrease to 63% of its original value. Adaptation during a mechanical stimulus was observable in *c-Kit*$^{-/-}$ mice, and firing rates decreased by >50% at the end of a 10 second static displacement stimulus in control and *c-Kit*$^{-/-}$ mice (Figure 43C). Time constants for SAM receptors in *c-Kit*$^{+/+}$ and *c-Kit*$^{-/-}$ were 1.83 and 2.67 seconds, respectively.

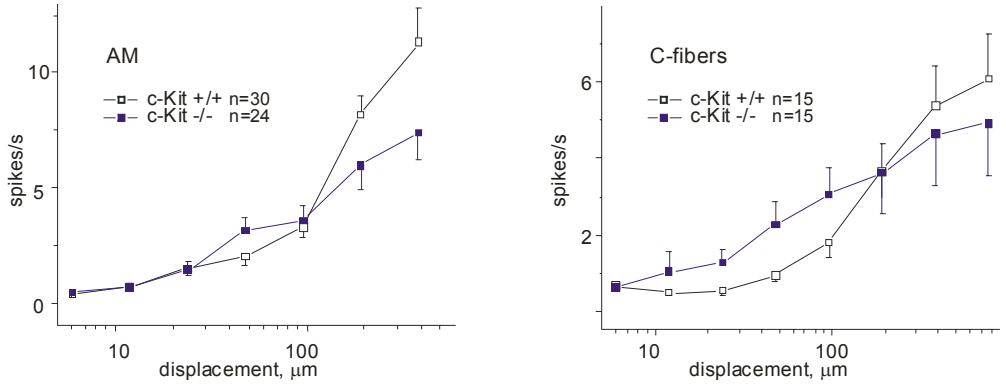

Figure 44. Mechanosensitivity of mechanonociceptors in *c-Kit*$^{-/-}$ mice
Stimulus response function of AMs (left) and C-fibers (right). No significant differences were observed. Error bars indicate s.e.m.

The stimulus response function of mechanonociceptors was recorded. AMs from *c-Kit*$^{-/-}$ mice did not show any difference compared to control (Figure 44A). Also, there was no statistically significant difference in the discharge frequency of C-fiber mechanonociceptors in *c-Kit*$^{-/-}$ compared to *c-Kit*$^{+/+}$ mice (Figure 44B).

Examining of von Frey threshold also revealed altered sensitivity of receptors to mechanical stimuli in c-Kit mutant (Table 5). The *c-Kit*$^{-/-}$ SAM exhibited a lower von Frey threshold compared to controls (Figure 45A). Median vFT in *c-Kit*$^{-/-}$ was 1 mN and 1.4 mN in control mice (p=0.0002, Mann-Whitney U test). AM units also have lower median von Frey thresholds compared to *c-Kit*$^{+/+}$, 2.5 mN and 3.6 mN respectively (p=0.0315, Mann-Whitney U test) (Figure 45B). In the other types of fibers examined (RAM, D-hair, C-fibers) there was no difference in von Frey threshold compared to controls.

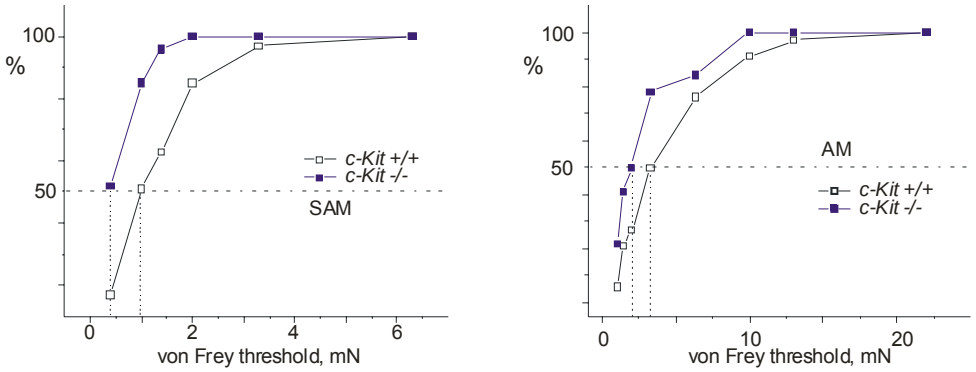

Figure 45. Von Frey threshold of mechanically sensitive receptors in *c-Kit*$^{-/-}$ mice
Mechanical threshold was examined in *c-Kit*$^{-/-}$ mice. Low threshold mechanoreceptors, SAM, (left) and high threshold mechanonociceptors, AM, (right panel) exhibited higher mechanical sensitivity having lower median vFT (p=0.0002, p=0.0315, respectively, Mann-Whitney U test).

Thermal sensitivity in *c-Kit*$^{-/-}$ mice

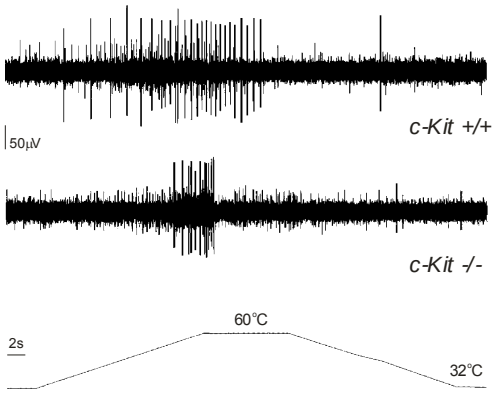

Figure 46. Electrophysiological analysis of sensory neurons in control and *c-Kit*$^{-/-}$ mice
Representative traces of single unit recording from a *c-Kit*$^{+/+}$ mice (upper panel) and *c-Kit*$^{-/-}$ mice (lower panel) to a heat stimulus applied to the skin.

The response of CMH fibers to noxious heat was analyzed in *c-Kit* mutants and decreased noxious heat sensitivity was observed (Figure 46). The average temperature threshold for the first AP evoked by the heat stimulus was 47.21±1.88°C, significantly higher than in control mice, 40.27±1.20°C (p=0.0016, unpaired T test) (Figure 47A). The same was for the second AP; 50.52±1.64°C for *c-Kit*$^{-/-}$ and 43.34±1.29 for *c-Kit*$^{+/+}$ (p=0.0009, unpaired T test) (Figure 47A). The noxious heat threshold in the mutant was therefore elevated by 7°C. Furthermore, *c-Kit* mutants displayed a large reduction in firing rate upon stimulation with standardized heat ramp (p<0.0001, two way ANOVA) (Figure 47B). The average total number of spikes from CMH fibers in *c-Kit*$^{-/-}$ was 3.6 fold smaller than found in control neurons (14.08±2.52 in c-Kit mutant compared to 51.04±9.28 in controls). Thus, a phenotype characteristic for anti-NGF treated mice was found in mice carrying *c-Kit* null mutation. *c-Kit*$^{-/-}$ noxious heat sensitivity was even more affected compared to neonataly anti-NGF deprived mice.

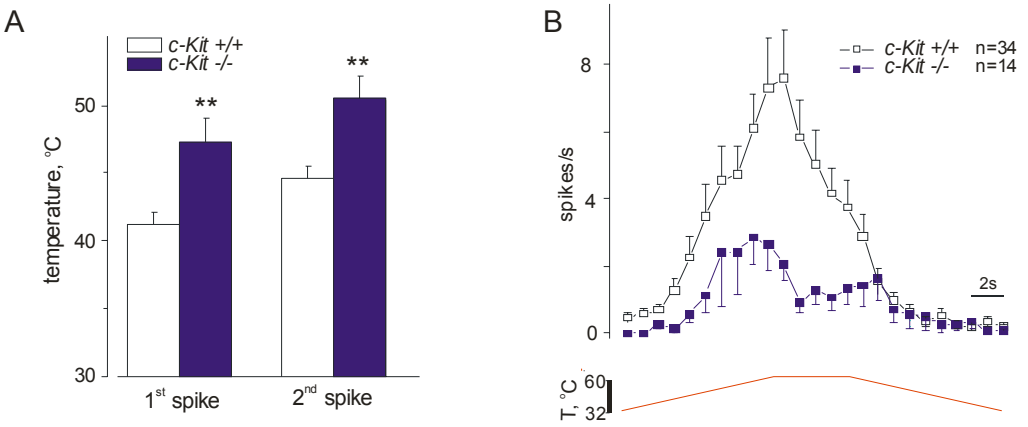

Figure 47. Effect of *c-Kit* null mutation on heat sensitivity of CMH
A The onset temperature for the first and the second action potential was measured for control and *c-Kit*$^{-/-}$ mice. The mutation induced a change in the thermal threshold. The threshold temperature was 7°C higher for both first (p=0.0016, unpaired t test) and a second (p=0.0009, unpaired t test) action potentials in *c-Kit*$^{-/-}$ mice. B Heat response function. CMH of *c-Kit*$^{-/-}$ mice displayed significantly lower firing rate to heat ramp (p<0.0001, two way ANOVA). Error bars indicate s.e.m.

Decreased heat sensitivity was also manifested at a behavioral level. *c-Kit*$^{-/-}$ mice demonstrated a marked hypoalgesia to radiant heat applied to the hind paw with an average increase of 40% for foot withdrawal latency compared to controls (Figure 48A).

In contrast, the foot withdrawal latency to punctuate mechanical stimuli was 20% decreased (Figure 48B). Thus, mice lacking c-Kit function displayed relatively mild mechanical hyperalgesia and profound heat hypoalgesia compared to the control. (Behavioral tests for thermal and mechanical nociception were carried out together with Christina Fhram)

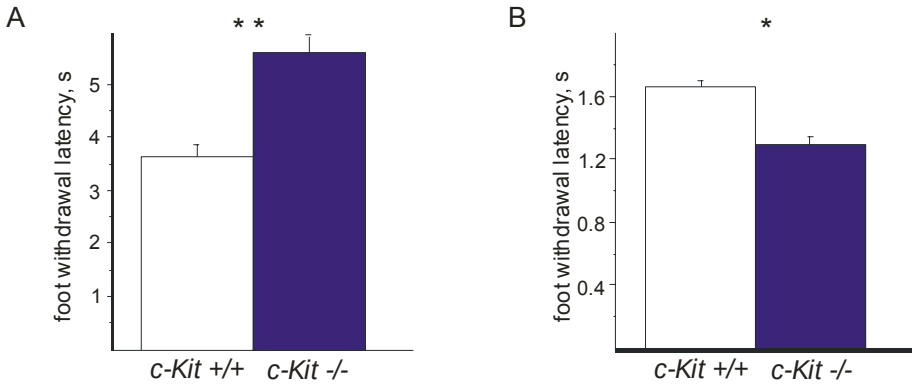

Figure 48. *c-Kit* null mutation led to behavioral thermal hypoalgesia and mechanical hyperalgesia
A Heardgraeves test was employed to measure the hind paw withdrawal latency. The paw withdrawal latency to noxious heat was significantly longer in *c-Kit*$^{-/-}$ mice ($p<0.0001$, unpaired t test). B There was also a significant difference in the paw withdrawal latency to noxious mechanical stimulus ($p=0.0001$, unpaired t test). Error bars indicate s.e.m. (Behavioral tests for thermal and mechanical nociception were done together with Christina Fhram).

Heat sensitivity is impaired in c-Kit heterozygote

The properties of C-fiber nociceptors in *c-Kit*$^{+/-}$ mice were also analyzed to test if the functional deficit in C-fibers is observed with *c-Kit* haploinsufficiency. Interestingly, a reduction in noxious heat sensitivity of CMH fibers in *c-Kit*$^{+/-}$ mice was quantitatively indistinguishable from that observed in *c-Kit*$^{-/-}$ mice (Figure 49A-B). The heat threshold for the first AP evoked by the heat stimulus was 47.25±2.30^{o}C, significantly higher than in control mice and comparable to *c-Kit*$^{-/-}$ mice ($p=0.0044$, unpaired T test) (Figure 49A). The same was for the second AP, the threshold temperature in *c-Kit*$^{+/-}$ mice was

50.15±1.89°C (p=0.0039 compared to control, unpaired T test) (Figure 49A). The heat response curve in *c-Kit*$^{+/-}$ was also very similar to *c-Kit*$^{-/-}$, although slightly higher (Figure 49B). In contrast to the phenotype observed in CMH fibers there was no indication that *c-Kit* haploinsufficiency produced changes in mechanoreceptors. The relative proportion of SAM and RAM fibers remained similar to control, as well as the SAM response to mechanical displacements (Figure 49D).

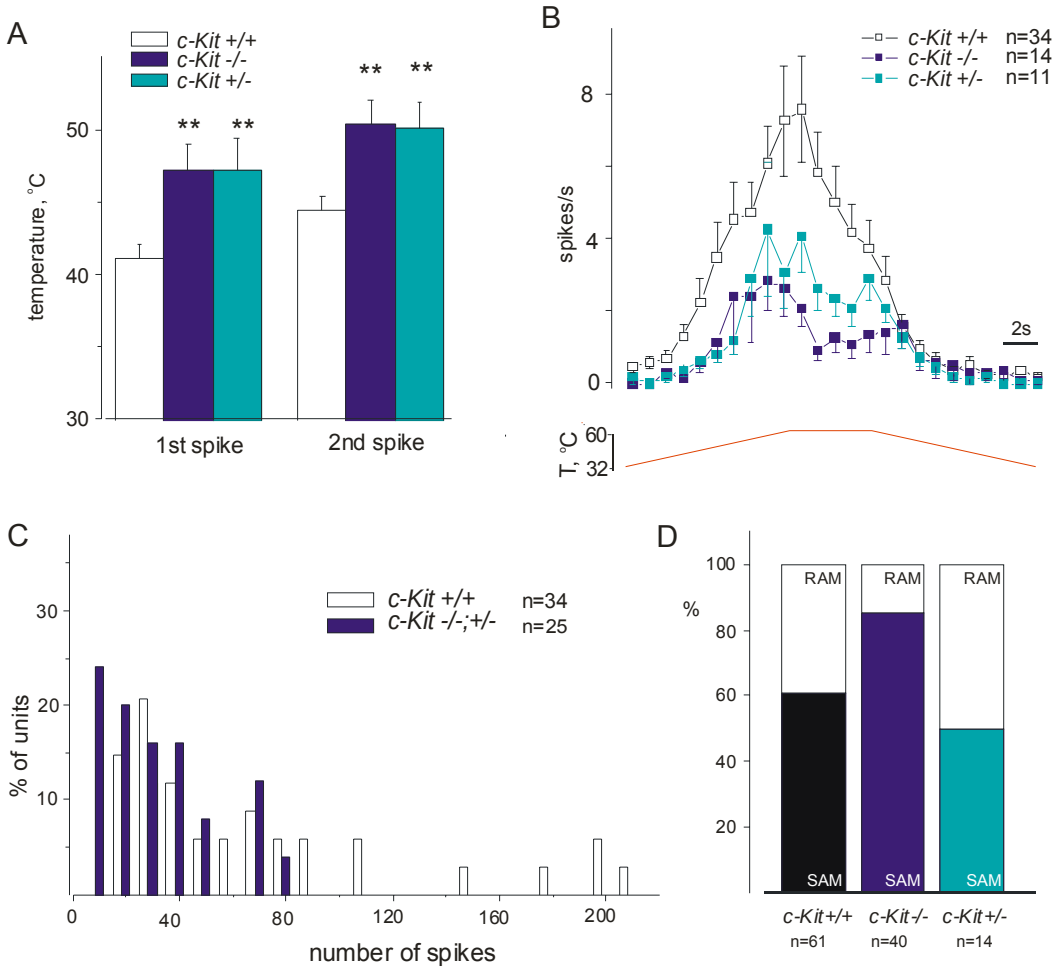

Figure 49. Effect of *c-Kit* haploinsufficiency on heat sensitivity of CMH
A The haploinsufficiency increased the thermal threshold in *c-Kit*$^{+/-}$ mice. The threshold temperature was 7°C higher for both first and the second action potentials compared to control mice and indistinguishable from *c-Kit*$^{-/-}$ CMH thresholds. B The heat response function of *c-Kit*$^{+/-}$ CMH fibers is similar to *c-Kit*$^{-/-}$ and lower compared to heat response of control mice. Error bars indicate s.e.m. C The distribution of the total heat response of individual units in control and *c-Kit*$^{-/-;+/-}$ mice. The high responding CMH units are missing in *c-Kit* deficient mice. D *c-Kit* haploinsufficiency did not alter the relative proportion of Aβ mechanoreceptors.

To further analyze the influence of *c-Kit* insufficiency on CMH the distribution of the total heat response of individual units in control and *c-Kit*$^{-/-;+/-}$ mice was plotted (Figure 49C). Among control CMH around 50% of units fired more than 80 spikes upon heat ramp, some of them reaching more than 200 spikes per stimulus. In contrast, none of the *c-Kit*$^{-/-;+/-}$ CMH units had total number of spikes over 80 (Figure 49C). Those CMH fibers with high heat response ("high responders", >60 spikes/stimulus) were essentially absent in *c-Kit* mutants. This data suggests that a subpopulation of "high responding" CMH fibers require c-Kit signaling to maintain their normal noxious heat sensitivity.

The heat current is potentiated by c-Kit ligand

The *c-Kit* mutation had very profound effect on noxious heat sensitivity. To test whether c-Kit signaling acutely sensitizes the noxious heat activated currents (I_{heat}) whole cell recordings from small diameter sensory neurons were performed and SCF, the c-Kit ligand, was used to try and evoke sensitization.

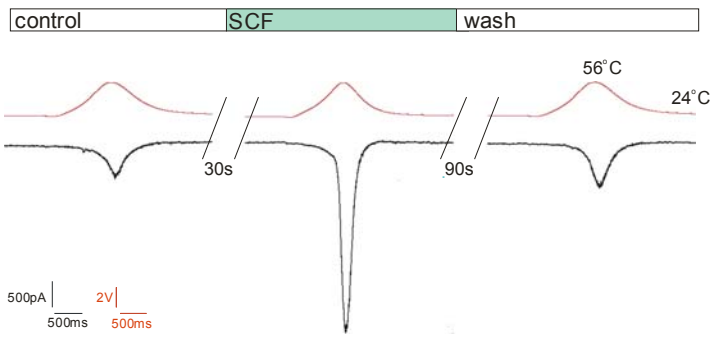

Figure 50. Potentiation of I_{heat} in DRG neurons by c-Kit ligand SCF
Electrophysiological analysis of I_{heat} in cultivated small diameter sensory neurons was performed. SCF application during the heat stimulus resulted in potentiation of I_{heat} in approximately 50% of cells with a heat gated current. The effect of SCF was reversible. Recorded inward current (black trace) in response to a standard heat stimulus (red trace) before, during addition of SCF, and after washout.

DRG neurons from adult mice were cultured and experiment performed 24-48 h after plating. Heat ramp stimuli from 24 to 56°C were applied using an automated perfusion system WAS02 enabling drug application concomitantly with local cell heating. I_{heat} was recorded before, during and after application of 10 nM SCF. Transiently applied heat stimuli typically resulted in inward currents of 200-500 pA (Figure 50). In a single cell, repeated heating resulted in identical heat activated currents without any evidence of tachyphylaxis. However, within 30 seconds after application of SCF, about half the thermoreceptive neurons displayed potentiation of I_{heat} (Figure 51).

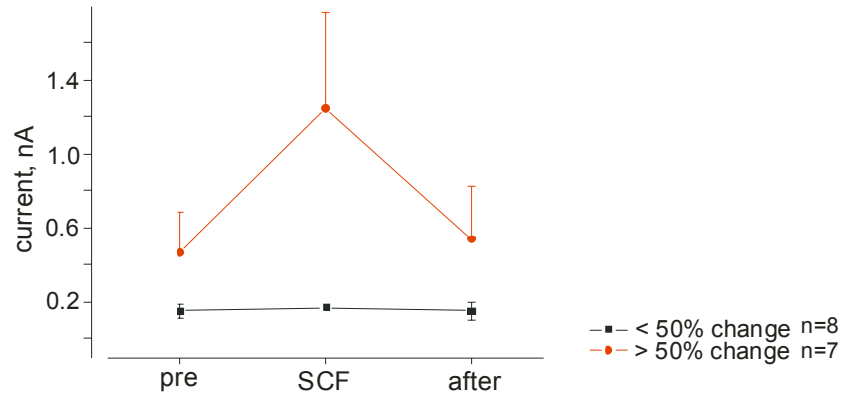

Figure 51. Approximately 50% of heat sensitive cultivated DRG cells were affected by SCF application
Quantification of heat-induced inward currents distinguished two neuronal populations, one that showed robust potentiation of I_{heat} in response to SCF, depicted in red ($p<0.01$, Wilcoxin test on ranks), and another cell population that was unresponsive to SCF, depicted in black. Error bars indicate s.e.m.

Two populations of thermoreceptive neurons could therefore be distinguished; one was unresponsive to SCF (defined as less than 50% change in I_{heat} during SCF stimulation), and the other showed a potentiation of the heat-dependent inward current (more than 50% increase in heat-induced inward current during SCF application). SCF responsive nociceptors made up approximately 50% of the cells tested, and responsive cells tended to be those with larger initial I_{heat} amplitudes (Figure 51). The mean I_{heat} of unresponsive cells was 150.8±36.6 pA and 467.8±221.4 pA for cells that were potentiated by SCF. After potentiation mean I_{heat} was 1248.3±515.1 pA, in average 2.7

fold higher then prior and after SCF application (Figure 51). The effect of SCF was short lasting, and was not detectable 90 seconds after washout (Figure 50). In some cases SCF was applied a few times, washing-out between applications, and it was possible to repeatedly induce potentiation with recovery of I_{heat} to control values after each washout. SCF did not only lead to a clear increase in the amplitude of I_{heat}, but also produced a lowering of the heat threshold by approximately 1.8°C (Figure 52). Nevertheless, due to a very short lasting heat ramp it was difficult to read out the exact values of I_{heat} temperature threshold.

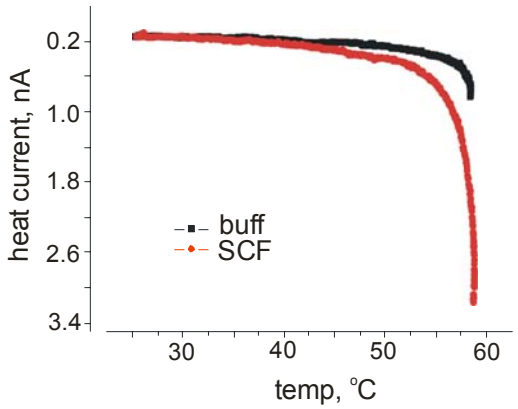

Figure 52. SCF alters the threshold temperature of I_{heat}
Representative trace of inward current magnitude plotted against temperature for a single SCF-responsive cell, prior to (black trace) and during SCF application (red trace).

Summary

c-Kit is expressed in small diameter and a subpopulation of big diameter neurons in DRG. It appears that *c-Kit* has a crucial role in setting the heat sensitivity in unmyelinated mechanonociceptors and mechanical sensitivity of a distinct class of low threshold mechanoreceptors. SAM fibers in *c-Kit*$^{-/-}$ mice displayed hypersensitivity to mechanical stimuli. Concerning heat sensitivity, mice carrying *c-Kit* null mutation have a phenotype very similar to that observed in anti-NGF treated mice. *c-Kit*$^{-/-}$ mice displayed profound noxious heat hyposensitivity: the thermal threshold was elevated; the discharging frequency upon heat ramp stimulus was reduced in CMH fibers; and *c-Kit*$^{-/-}$ mice were also behaviorally hypoalgesic to thermal stimuli. Furthermore, the c-Kit ligand SCF, was found to potentiate I_{heat} in subpopulation of small DRG neurons. The subpopulation of high frequency responding heat sensitive C fibers was missing in both *c-Kit*$^{-/-}$ and *c-Kit*$^{+/-}$ mice. Therefore, *c-Kit* seems to be important for control of the noxious heat sensitivity in a subpopulation of CMH fibers.